Chinese Journal of Aeronautics, (2014),27(5): 1273–1287

Chinese Society of Aeronautics and Astronautics
& Beihang University

Chinese Journal of Aeronautics

cja@buaa.edu.cn
www.sciencedirect.com

Fuzzy adaptive tracking control within the full envelope for an unmanned aerial vehicle

Liu Zhi, Wang Yong *

Department of Automation Science and Electrical Engineering, Beihang University, Beijing 100191, China

Received 10 September 2013; revised 4 March 2014; accepted 12 May 2014
Available online 6 September 2014

KEYWORDS

Flight control systems;
Full flight envelope;
Fuzzy adaptive tracking control;
Fuzzy multiple Lyapunov function;
Fuzzy T–S model;
Single hidden layer neural network

Abstract Motivated by the autopilot of an unmanned aerial vehicle (UAV) with a wide flight envelope span experiencing large parametric variations in the presence of uncertainties, a fuzzy adaptive tracking controller (FATC) is proposed. The controller consists of a fuzzy baseline controller and an adaptive increment, and the main highlight is that the fuzzy baseline controller and adaptation laws are both based on the fuzzy multiple Lyapunov function approach, which helps to reduce the conservatism for the large envelope and guarantees satisfactory tracking performances with strong robustness simultaneously within the whole envelope. The constraint condition of the fuzzy baseline controller is provided in the form of linear matrix inequality (LMI), and it specifies the satisfactory tracking performances in the absence of uncertainties. The adaptive increment ensures the uniformly ultimately bounded (UUB) predication errors to recover satisfactory responses in the presence of uncertainties. Simulation results show that the proposed controller helps to achieve high-accuracy tracking of airspeed and altitude desirable commands with strong robustness to uncertainties throughout the entire flight envelope.

1. Introduction

As the development of modern UAVs, the flight envelope is expanded constantly. Flight control confronts the challenge of high-precision tracking of desirable instruments with strong robustness for the entire flight envelope. A UAV is a multi-input, multi-output nonlinear system with strong coupling, and the aerodynamic forces and moments for the kinetics depend not only on the dynamic pressure but also on the force and moment coefficients as a function of aerodynamic derivatives. The engine thrust, dynamic pressure, and aerodynamic derivatives vary significantly along with the changes of Mach number and altitude, especially during a transonic flight. Therefore, the operating and stability characteristics of a UAV at different operating points vary remarkably.[1] In addition, undesirable uncertainties intensify the difficulty due to modeling errors, parametric perturbations, and control efficiency failures within the full envelope.

Although local model based robust control,[2] adaptive dynamic inversion control,[3] and L1 adaptive control[4] enhance performances, they are not applicable for a flight over a large envelope. The interpolation of local linearization-based

* Corresponding author. Tel.: +86 10 82317544.
E-mail address: wy_buaa@sina.com (Y. Wang).

Peer review under responsibility of Editorial Committe of CJA.

Production and hosting by Elsevier

http://dx.doi.org/10.1016/j.cja.2014.08.012

controllers in terms of flight condition is widely applied in engineering, but stability could not be guaranteed.[1] The gap metric[5] and guardian maps[6] approaches extend stability to the entire envelope iteratively, but the processes are time-consuming.

The linear parameter varying (LPV) control is a popular gain-scheduling approach for a large envelope. However, the conservatism of the common Lyapunov method based robust[7] or adaptive controllers[8,9] may lead to no feasible solution for desired performances. To relax the conservatism, Huang et al.[10] provided switching the LPV robust controller using multiple Lyapunov functions for air-breathing hypersonic vehicles, while Lu et al.[11] switched the LPV controller using hysteresis and average dwell time logics respectively. However, higher computational complexities emerge and they ensure robustness at the price of response performances. Hou et al.[12,13] enhanced the response performances with the adaptive increment, but dwell time restricts the arbitrary switching and switching dynamics may cause underlying damages.

The fuzzy control is also an attractive alternative for robust control within a full envelope.[14] The generalized fuzzy hybrid controllers blend the common Lyapunov function with $H\infty$,[15] the sliding mode,[16] or MRAC,[17] and they degrade control performances due to the conservatism. To reduce the conservatism, Feng[18] proposed a piecewise Lyapunov function based fuzzy $H\infty$ controller, but the switching dynamics could not be avoided. The fuzzy multiple Lyapunov functions can reduce the control conservatism with the advantage of a continuity feature,[19] and Bouarar et al.[20] reduced computational complexity by adopting the descriptor system approach, yet the local $H\infty$ controller guarantees robustness at the cost of response performances.[21] Although Wu and Juang[22] employed a fuzzy adaptive sliding-mode controller to relax the cost of response for robustness, chattering emerges owing to the discontinuous control signals across the sliding surfaces.

Based on the above analysis, a fuzzy multiple Lyapunov function based tracking controller augmenting a fuzzy baseline controller with an adaptive increment is proposed. The key breakthroughs can be concluded as follows:

(1) The conservatism of the fuzzy baseline controller and the adaptation law for the entire flight envelope is relaxed by employing the fuzzy multiple Lyapunov method.
(2) The computational complexity of LMI for the fuzzy baseline controller is reduced by using the descriptor system approach.
(3) The controller provides smooth control signals throughout the flight envelope.

2. Problem formation

2.1. Nonlinear kinetic model

The flight envelope[23] of a UAV refers to the capabilities of operating ranges in terms of Mach number and altitude. For a fix-wing UAV, the flight envelope is restricted by the stalling angle, service ceiling, maximum march, maximum dynamic pressure, performances of the engine, etc.

The original nonlinear model[23,24] in the path coordinate frame can be constructed as

$$\begin{cases} \dot{V}_{\mathrm{T}} = (T\cos(\alpha+\varphi) - D - mg\sin\gamma)/m \\ \dot{\gamma} = (T\sin(\alpha+\varphi) + L - mg\cos\gamma)/(mV_{\mathrm{T}}) \\ \dot{q} = M/J_z \\ \dot{\theta} = q \\ \alpha = \theta - \gamma \\ \dot{H} = V_{\mathrm{T}}\sin\gamma \end{cases} \tag{1}$$

where V_{T}, α, q, θ, γ and H are the airspeed, angle of attack, pitch rate, pitch angle, path angle, and altitude, respectively; φ is the angle of the thrust line; m is the mass; g is the gravitational constant; J_z is the pitch moment of inertia; T, L, D and M are the engine thrust, lift, drag, and pitch moment[24] expressed as

$$\begin{cases} T = P(\delta_{\mathrm{th}}, Ma, H) \\ L = \bar{q}SC_L \\ D = \bar{q}SC_D \\ M = \bar{q}S\bar{c}C_M - e_{\mathrm{p}}T \end{cases} \tag{2}$$

with $P(\cdot)$ the thrust curve; δ_{th} the throttle setting; Ma the Mach number; $S, \bar{c}$ and e_{p} the wing area, wing mean geometric chord, and thrust eccentricity; $\bar{q} = 0.5\rho(H)V_{\mathrm{T}}^2$ the dynamic pressure, and $\rho(H) = 1.225\ (1 - H/44331)^{4.25588}$ the air density; and C_L,C_D, C_M the lift, drag, and pitching moment coefficients defined by

$$\begin{cases} C_L = C_{L\alpha}Ma(\alpha - \underline{\alpha}) + C_{L\delta_{\mathrm{e}}}Ma\delta_{\mathrm{e}} \\ C_D = AMaC_L^2 + C_{D0}Ma \\ C_M = C_{M0}Ma + \left(x_{\mathrm{cgR}} - x_{\mathrm{caR}}Ma\right)C_L \\ \qquad + C_{M\delta_{\mathrm{e}}}Ma\delta_{\mathrm{e}} + \dfrac{C_{Mq}Maq\bar{c}}{V_{\mathrm{T}}} + \dfrac{C_{M\dot{\alpha}}Ma\dot{\alpha}\bar{c}}{V_{\mathrm{T}}} \end{cases} \tag{3}$$

where $\underline{\alpha}$ is the zero lift angle; δ_{e} is the elevator deflections; $\dot{\alpha}$ is the derivative of the angle of attack; $C_{L\alpha}, C_{L\delta_{\mathrm{e}}}, A, C_{D0}, C_{M0}, C_{M\delta_{\mathrm{e}}}, C_{Mq}$, and $C_{M\dot{\alpha}}$ are the aerodynamic derivatives; and x_{cgR} x_{caR} are the reference locations of the gravity and aerodynamic centers.

The relationship between the flight of a UAV over a large envelope and the nonlinear kinetics can be illustrated in Fig. 1. As shown in Fig. 1, the thrust and aerodynamic derivatives connect the operating points in the flight envelope with the forces and moments in the nonlinear model. The natural frequency and damp of short-period and phugoid-period vary remarkably along with airspeed, altitude, dynamic pressure, and aerodynamic derivatives.[24] Hence, we can use the Mach number and the altitude as the premise variables to distinguish the natural characteristics of the UAV over a large flight envelope.[1]

2.2. Fuzzy T–S model

As the fuzzy system with the Gaussian membership function has been shown to realize the universal approximation of any nonlinear functions on the considered compact set,[25] the nonlinear model of Eq. (1) can be transformed to an uncertain fuzzy T–S system as

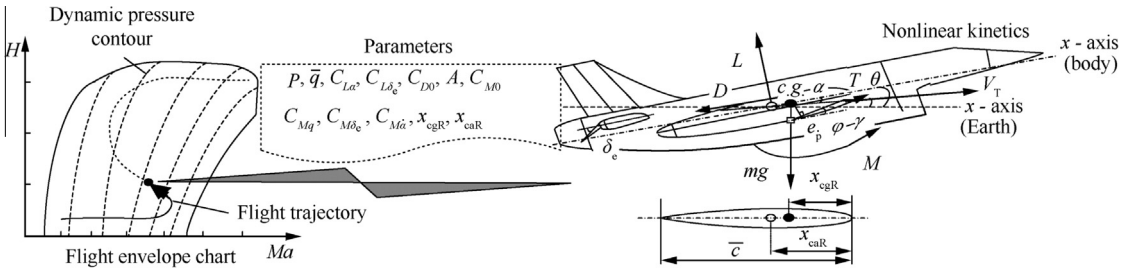

Fig. 1 Relationship between flight of a UAV over a large envelope and nonlinear kinetics.

$$\begin{cases} \dot{\boldsymbol{x}}(t) = \sum_{i=1}^{N}\mu_i(\boldsymbol{z}(t))\boldsymbol{A}_i\boldsymbol{x}(t) + \sum_{i=1}^{N}\mu_i(\boldsymbol{z}(t))\boldsymbol{B}_i \\ \qquad \times\left[\left(\boldsymbol{I}+\boldsymbol{\Lambda}^{\mathrm{T}}(t)\right)\boldsymbol{u}(t) + \boldsymbol{L}(\boldsymbol{x}(t),\boldsymbol{z}(t))\right] \\ \boldsymbol{y}(t) = \sum_{i=1}^{N}\mu_i(\boldsymbol{z}(t))\boldsymbol{C}_i\boldsymbol{x}(t) \end{cases} \tag{4}$$

where $\boldsymbol{x}(t) = [V_{\mathrm{T}}, \alpha, q, \theta, H]^{\mathrm{T}}$, $\boldsymbol{u}(t) = [\delta_{\mathrm{th}}, \delta_{\mathrm{e}}]^{\mathrm{T}}$ and $\boldsymbol{y}(t) = [V_{\mathrm{T}}, H]^{\mathrm{T}}$ denote the system state, input, and output vectors, respectively; N is the size of the fuzzy rules; $\boldsymbol{z}(t) = [z_1(t), z_2(t)]^{\mathrm{T}}$ is the premise variable and $z_1(t) = Ma$, $z_2(t) = H$; $\boldsymbol{L}(\boldsymbol{x}(t), \boldsymbol{z}(t))$ represents the modeling errors and unknown parametric perturbations; $\boldsymbol{\Lambda}(t) = \mathrm{diag}(\Lambda_1(t),\Lambda_2(t))$ is the unknown diagonal matrix with $\Lambda_1(t)$ and $\Lambda_2(t)$ modeling the control efficiency failures of thrust and elevator; $\boldsymbol{A}_i \in \mathbf{R}^{5\times5}$, $\boldsymbol{B}_i \in \mathbf{R}^{5\times2}$, $\boldsymbol{C}_i \in \mathbf{R}^{2\times5}$ ($i = 1, 2, \ldots, N$) are the local system matrices; $\mu_i(\boldsymbol{z}(t)) \geqslant 0$ is the membership degree defined as

$$\begin{cases} \mu_i(\boldsymbol{z}(t)) = \prod_{k=1}^{K} f_k^i(z_k(t)) \Big/ \sum_{i=1}^{N}\left(\prod_{k=1}^{K} f_k^i(z_k(t))\right) \\ \sum_{i=1}^{N}\mu_i(\boldsymbol{z}(t)) = 1 \end{cases} \tag{5}$$

with $f_k^i(z_k(t))$ the ith Gaussian membership function of $z_k(t)$ reflecting to the fuzzy set Z_k^i, and

$$f_k^i(z_k(t)) = \exp\left[\frac{-\left(z_k(t) - \bar{z}_k^i\right)^2}{\sigma_k^{i\,2}}\right] \tag{6}$$

where $\bar{z}_k^i$ and σ_k^i are the center and width of $f_k^i(z_k(t))$. Note that we set symbols $n = 5$, $\bar{m} = 2$, $K = 2$ to represent the sizes of the system states, inputs, and premise variables, respectively.

For any $i = 1, 2, \ldots, N$ and $k = 1, 2$, the parameters $\bar{z}_k^i$ and σ_k^i are obtained through the orthogonal projection of fuzzy partition, which is realized by fuzzy c-means clustering of flight dynamics.[14,26] $\boldsymbol{A}_i$, $\boldsymbol{B}_i$ and $\boldsymbol{C}_i$ ($i = 1, 2, \ldots, N$) are acquired via local linearization with respect to the centers of the fuzzy rules. The overlapped membership degrees of the fuzzy partition matrix renders the universe of discourse of the Gaussian membership function to exceed the boundary of the flight envelope, so the dynamics of the fuzzy T–S system can cover the flight envelope region sufficiently with N overlapped ellipses. [27]

Assumption 1. The flight envelope constrains that $\boldsymbol{z}(t)$ belongs to the compact set $\boldsymbol{\Omega}_z$.

Assumption 2. The uncertainties $\boldsymbol{L}(\boldsymbol{x}(t), \boldsymbol{z}(t))$ can be approximated by a single hidden layer neural network (SHLNN) over the compact set $(\boldsymbol{x}(t), \boldsymbol{z}(t)) \in \boldsymbol{\Omega}_x \times \boldsymbol{\Omega}_z$ with a known structure and size as[28]

$$\begin{cases} \boldsymbol{L}(\boldsymbol{x}(t),\boldsymbol{z}(t)) = \boldsymbol{W}^{\mathrm{T}}\boldsymbol{\sigma}\left(\boldsymbol{V}^{\mathrm{T}}\boldsymbol{\psi}(t)\right) + \boldsymbol{\varepsilon}(\boldsymbol{\psi}(t)) \\ \|\boldsymbol{\varepsilon}(\boldsymbol{\psi}(t))\| \leqslant \bar{\varepsilon} \end{cases} \tag{7}$$

where $\boldsymbol{\psi}(t) = [b_\sigma, \boldsymbol{x}^{\mathrm{T}}(t), \boldsymbol{z}^{\mathrm{T}}(t)]^{\mathrm{T}}$ is the input; $\boldsymbol{W} \in \mathbf{R}^{(l+1)\times\bar{m}}$, $\boldsymbol{V} \in \mathbf{R}^{(n+K+1)\times l}$ are unknown connection weights of SHLNN; $\boldsymbol{\sigma}(\boldsymbol{V}^{\mathrm{T}}\boldsymbol{\psi}(t)) = [1, \sigma_1(\boldsymbol{v}_1^{\mathrm{T}}\boldsymbol{\psi}(t)), \sigma_2(\boldsymbol{v}_2^{\mathrm{T}}\boldsymbol{\psi}(t)), \ \ldots, \sigma_l(\boldsymbol{v}_l^{\mathrm{T}}\boldsymbol{\psi}(t))]^{\mathrm{T}} \in \mathbf{R}^{l+1}$ is the hidden layer operation; $b_\sigma = 1$ is the input bias; l is the size of the hidden layer neuron; $\boldsymbol{v}_i (i = 1, 2, \ldots, l)$ is the ith column of matrix $\boldsymbol{V}$ satisfying $\|\boldsymbol{v}_i\| \leqslant \bar{v}_i$; $\boldsymbol{w}_i (i = 1, 2, \ldots, m)$ is the ith column of $\boldsymbol{W}$ satisfying $\|\boldsymbol{w}_i\| \leqslant \bar{w}_i$, where $\bar{v}_i$ and $\bar{w}_i$ are constant values determined according to the range of uncertainty; $\boldsymbol{\varepsilon}(\boldsymbol{\psi}(t))$ is the approximated error vector with the upper bound $\bar{\varepsilon}$, and the basis function

$$\sigma_i\left(\boldsymbol{v}_i^{\mathrm{T}}\boldsymbol{\psi}(t)\right) = \frac{1}{1+\exp\left(-a_i\boldsymbol{v}_i^{\mathrm{T}}\boldsymbol{\psi}(t)\right)} \quad (i = 1, 2, \ldots, l) \tag{8}$$

with $a_i > 0$ ($i = 1, 2, \ldots, l$) the activation potential factor. And $\|\cdot\|$ denotes the 2-norm of the matrix.

Assumption 3. The control efficiency failures are constrained as

$$\begin{cases} |\Lambda_i(t)| < \bar{\Lambda}_i \\ |\dot{\Lambda}_i(t)| < d_{\Lambda i} \end{cases} (i = 1, 2) \tag{9}$$

where $0 < \bar{\Lambda}_i < 1$ and $d_{\Lambda i} > 0$ are known constants and satisfy $\bar{\Lambda}_1 + \bar{\Lambda}_2 < 1$.

Assumption 4. The membership degrees are continuously differentiable and slowly varying, i.e.,

$$|\dot{\mu}_i(\boldsymbol{z}(t))| \leqslant \phi_i \quad (i = 1, 2, \ldots, N-1) \tag{10}$$

where $\phi_i (i = 1, 2, \ldots, N-1)$ are known constants, and we define $\boldsymbol{\beta} = [\phi_1, \phi_2, \ldots, \phi_{N-1}]^{\mathrm{T}}$.

For simplicity, we use μ_i to represent $\mu_i(\boldsymbol{z}(t))$.

2.3. Control objective

The control objective is the precise tracking of airspeed and altitude commands with strong robustness within the full flight envelope. The desirable responses are specified by a command filter

$$\begin{cases} \dot{\boldsymbol{x}}_{\mathrm{c}}(t) = \boldsymbol{A}_{\mathrm{c}}\boldsymbol{x}_{\mathrm{c}}(t) + \boldsymbol{B}_{\mathrm{c}}\boldsymbol{r}(t) \\ \boldsymbol{y}_{\mathrm{c}}(t) = \boldsymbol{C}_{\mathrm{c}}\boldsymbol{x}_{\mathrm{c}}(t) \end{cases} \tag{11}$$

where $\boldsymbol{x}_{\mathrm{c}}(t) = [V_{\mathrm{Tc}}, \ \dot{V}_{\mathrm{Tc}}, \ H_{\mathrm{c}}, \ \dot{H}_{\mathrm{c}}]^{\mathrm{T}}$, $\boldsymbol{r}(t) = [V_{\mathrm{Tg}}, H_{\mathrm{g}}]^{\mathrm{T}}$, $\boldsymbol{y}_{\mathrm{c}}(t) = [V_{\mathrm{Tc}}, H_{\mathrm{c}}]^{\mathrm{T}}$; V_{Tg} and H_{g} are the given airspeed and altitude inputs; V_{Tc} and H_{c} are the desirable commands; and $\boldsymbol{A}_{\mathrm{c}}$, $\boldsymbol{B}_{\mathrm{c}}$,

$\boldsymbol{C}_c$ are the system matrices. $\boldsymbol{r}(t)$ is uniformly bounded. To remove steady-state errors, we define

$$\boldsymbol{d}(t)=\int_0^t(\boldsymbol{y}_c(\tau)-\boldsymbol{y}(\tau))\mathrm{d}\tau \tag{12}$$

With the augmentation of the command filter, the extended tracking system can be constructed as

$$\begin{aligned}\dot{\bar{\boldsymbol{x}}}(t)=&\sum_{i=1}^{N}\mu_i\overline{\boldsymbol{A}}_i\bar{\boldsymbol{x}}(t)+\sum_{i=1}^{N}\mu_i\overline{\boldsymbol{B}}_i\left[\left(\boldsymbol{I}_{\bar{m}}+\boldsymbol{\Lambda}^{\mathrm{T}}(t)\right)\times\boldsymbol{u}(t)\right.\\&\left.+\boldsymbol{L}(\boldsymbol{x}(t),\boldsymbol{z}(t))\right]+\overline{\boldsymbol{G}}\boldsymbol{r}(t)\end{aligned} \tag{13}$$

where $\bar{\boldsymbol{x}}(t)=\left[\boldsymbol{x}^{\mathrm{T}}(t),\boldsymbol{x}_c^{\mathrm{T}}(t),\boldsymbol{d}^{\mathrm{T}}(t)\right]^{\mathrm{T}}\in\mathbf{R}^{\bar{n}}$ with $\bar{n}=n+3\bar{m}$, $\boldsymbol{I}_{\bar{m}}$ is a unit matrix of dimension $\bar{m}$, and

$$\overline{\boldsymbol{A}}_i=\begin{bmatrix}\boldsymbol{A}_i&\boldsymbol{0}&\boldsymbol{0}\\\boldsymbol{0}&\boldsymbol{0}&\boldsymbol{A}_c\\-\boldsymbol{C}_i&\boldsymbol{0}&\boldsymbol{C}_c\end{bmatrix},\ \overline{\boldsymbol{B}}_i=\begin{bmatrix}\boldsymbol{B}_i\\\boldsymbol{0}\\\boldsymbol{0}\end{bmatrix},\ \overline{\boldsymbol{G}}=\begin{bmatrix}\boldsymbol{0}&\boldsymbol{0}\\\boldsymbol{0}&\boldsymbol{B}_c\\\boldsymbol{0}&\boldsymbol{0}\end{bmatrix}\qquad(i=1,2,\ldots,N)$$

3. Fuzzy adaptive tracking control for a UAV within the full envelope

Consider the following control law

$$\boldsymbol{u}(t)=\boldsymbol{u}_L(t)+\boldsymbol{u}_A(t) \tag{14}$$

where $\boldsymbol{u}_L(t)$ is the fuzzy baseline controller and $\boldsymbol{u}_A(t)$ is the adaptive increment. The fuzzy baseline controller specifies the satisfactory tracking performances in the absence of uncertainties, while the adaptive increment copes with the uncertainties to recover the specified tracking performances.

3.1. Fuzzy baseline controller

Define the quadratic performance index as

$$J=\int_0^{T_f}\left(\bar{\boldsymbol{x}}^{\mathrm{T}}(t)\boldsymbol{Q}\bar{\boldsymbol{x}}(t)+\boldsymbol{u}^{\mathrm{T}}(t)\boldsymbol{R}\boldsymbol{u}(t)\right)\mathrm{d}t \tag{15}$$

where $\boldsymbol{Q}$ and $\boldsymbol{R}$ are the given diagonal positive matrices, and T_f is the terminal time.

Applying the fuzzy multiple Lyapunov function approach, we introduce the fuzzy baseline controller

$$\boldsymbol{u}_L(t)=-\sum_{i=1}^{N}\mu_i\overline{\boldsymbol{K}}_i\bar{\boldsymbol{x}}(t)=-\sum_{i=1}^{N}\mu_i\underbrace{\boldsymbol{N}_i\left(\sum\nolimits_{j=1}^{N}\mu_j\boldsymbol{X}_j\right)^{-1}}_{\overline{\boldsymbol{K}}_i}\bar{\boldsymbol{x}}(t) \tag{16}$$

where $\boldsymbol{X}_j\in\mathbf{R}^{\bar{n}\times\bar{n}}(j=1,2,\ldots,N)$ is the jth Lyapunov positive define matrix, $\boldsymbol{N}_i\in\mathbf{R}^{\bar{m}\times\bar{n}}$ and $\overline{\boldsymbol{K}}_i\in\mathbf{R}^{\bar{m}\times\bar{n}}$ are the ith (i = 1, 2,…, N) local proportional matrix and the composited gain matrix, respectively.

In the absence of uncertainties, the extended tracking system of Eq. (13) with $\boldsymbol{u}_L(t)$ takes the form of

$$\dot{\bar{\boldsymbol{x}}}(t)=\sum_{i=1}^{N}\mu_i\left(\overline{\boldsymbol{A}}_i+\overline{\boldsymbol{B}}_i\sum_{j=1}^{N}\mu_j\overline{\boldsymbol{K}}_j\right)\bar{\boldsymbol{x}}(t)+\overline{\boldsymbol{G}}\boldsymbol{r}(t) \tag{17}$$

and it can be represented in the form of an equivalent descriptor system

$$\widehat{\boldsymbol{E}}\dot{\widehat{\boldsymbol{x}}}(t)=\sum_{i=1}^{N}\mu_i\widehat{\boldsymbol{A}}_i\widehat{\boldsymbol{x}}(t)+\widehat{\boldsymbol{G}}\boldsymbol{r}(t) \tag{18}$$

where

$$\begin{cases}\widehat{\boldsymbol{x}}(t)=\begin{bmatrix}\bar{\boldsymbol{x}}(t)\\\boldsymbol{u}_L(t)\end{bmatrix}\\\widehat{\boldsymbol{E}}=\begin{bmatrix}\boldsymbol{I}_{\bar{n}}&\boldsymbol{0}\\\boldsymbol{0}&\boldsymbol{0}\end{bmatrix}\\\widehat{\boldsymbol{A}}_i=\begin{bmatrix}\overline{\boldsymbol{A}}_i&\overline{\boldsymbol{B}}_i\\-\overline{\boldsymbol{K}}_i&\boldsymbol{I}_{\bar{m}}\end{bmatrix}\\\widehat{\boldsymbol{G}}=\begin{bmatrix}\overline{\boldsymbol{G}}\\\boldsymbol{0}\end{bmatrix}\end{cases}\qquad(i=1,2,\ldots,N)$$

Theorem 1. *Under Assumptions* 1–4, *for a given quadratic performance index defined as* Eq. (15) *and a descriptor system given by* Eq. (18), *if there exists a feasible solution* $(\boldsymbol{X}_i,\boldsymbol{X}_{21i},\boldsymbol{X}_{22i},\boldsymbol{N}_i,\chi^2)|_{i=1,2,\ldots,N}$ *satisfying*

$$\begin{cases}\boldsymbol{\Theta}_{ii}\leqslant\boldsymbol{0}&(i=1,2,\ldots,N)\\\dfrac{1}{N-1}\boldsymbol{\Theta}_{ii}+\dfrac{1}{2}\left(\boldsymbol{\Theta}_{ij}+\boldsymbol{\Theta}_{ji}\right)\leqslant\boldsymbol{0}&(1\leqslant i\neq j\leqslant N)\\\boldsymbol{X}_N-\boldsymbol{X}_i>\boldsymbol{0}&(i=1,2,\ldots,N-1)\\\boldsymbol{X}_i=\boldsymbol{X}_i^{\mathrm{T}}>\boldsymbol{0}&(i=1,2,\ldots,N)\end{cases} \tag{19}$$

where

$$\begin{cases}\boldsymbol{\Theta}_{ij}=\begin{bmatrix}\widehat{\boldsymbol{\Psi}}_{ij}&*&*\\\widehat{\boldsymbol{X}}_j&-\widehat{\boldsymbol{Q}}^{-1}&*\\\widehat{\boldsymbol{G}}^{T}&\boldsymbol{0}&-\chi^2\boldsymbol{I}_{\bar{n}+\bar{m}}\end{bmatrix}\\\widehat{\boldsymbol{\Psi}}_{ij}=\begin{bmatrix}\left(\begin{array}{c}\boldsymbol{X}_j^{\mathrm{T}}\overline{\boldsymbol{A}}_i^{\mathrm{T}}+\boldsymbol{X}_{21j}^{\mathrm{T}}\overline{\boldsymbol{B}}_i^{\mathrm{T}}+\overline{\boldsymbol{A}}_i\boldsymbol{X}_j\\+\overline{\boldsymbol{B}}_i\boldsymbol{X}_{21j}+\sum_{\hbar=1}^{N-1}\phi_\hbar(\boldsymbol{X}_N-\boldsymbol{X}_\hbar)\end{array}\right)&*\\\boldsymbol{X}_{22j}^{\mathrm{T}}\overline{\boldsymbol{B}}_i^{\mathrm{T}}-\boldsymbol{N}_i+\boldsymbol{X}_{21j}&\boldsymbol{X}_{22j}^{\mathrm{T}}+\boldsymbol{X}_{22j}\end{bmatrix}\end{cases}$$

then $\boldsymbol{u}_L(t)$ *in* Eq. (16) *is a stabilizing controller rendering*

$$J\leqslant\bar{J}=\widehat{\boldsymbol{x}}_0^{\mathrm{T}}\bar{\boldsymbol{P}}_{v0}\widehat{\boldsymbol{x}}_0+\chi^2\int_0^{T_f}\boldsymbol{r}^{\mathrm{T}}(\tau)\boldsymbol{r}(\tau)\mathrm{d}\tau \tag{20}$$

where $\widehat{\boldsymbol{x}}_0=\widehat{\boldsymbol{x}}(t_0)$, $\chi>0$ *is the attenuation level, and*

$$\overline{\boldsymbol{P}}_{v0}=\left[\boldsymbol{I}_{\bar{n}\times\bar{n}}^{\mathrm{T}},\boldsymbol{0}_{\bar{m}\times\bar{n}}^{\mathrm{T}}\right]\left[\sum_{j=1}^{N}\mu_j(\boldsymbol{z}(t_0))\widehat{\boldsymbol{X}}_j\right]^{-1}\begin{bmatrix}\boldsymbol{I}_{\bar{n}\times\bar{n}}\\\boldsymbol{0}_{\bar{m}\times\bar{n}}\end{bmatrix}$$

and $\boldsymbol{X}_{21i}\in\mathbf{R}^{\bar{m}\times\bar{n}}$, $\boldsymbol{X}_{22i}\in\mathbf{R}^{\bar{m}\times\bar{m}}$ *are the relative matrices for the solution of controller parameters in* Eq. (16).

Proof. Consider the following candidate fuzzy multiple Lyapunov function[20]

$$V(\widehat{\boldsymbol{x}}(t))=\widehat{\boldsymbol{x}}^{\mathrm{T}}(t)\widehat{\boldsymbol{E}}^{\mathrm{T}}\widehat{\boldsymbol{P}}_v\widehat{\boldsymbol{x}}(t) \tag{21}$$

where $\widehat{\boldsymbol{P}}_v=\sum_{j=1}^{N}\mu_j\widehat{\boldsymbol{P}}_j=\widehat{\boldsymbol{X}}_v^{-1}=\left(\sum_{j=1}^{N}\mu_j\widehat{\boldsymbol{X}}_j\right)^{-1}$ with $\widehat{\boldsymbol{X}}_j,\widehat{\boldsymbol{P}}_j\in\mathbf{R}^{\bar{n}\times\bar{n}}(j=1,2,\ldots,N)$. $\widehat{\boldsymbol{P}}_v$ is the nonsingular matrix restricted by

$$\widehat{\boldsymbol{E}}^{\mathrm{T}}\widehat{\boldsymbol{P}}_v=\widehat{\boldsymbol{P}}_v^{\mathrm{T}}\widehat{\boldsymbol{E}}\geqslant\boldsymbol{0} \tag{22}$$

The constraint condition Eq. (22) holds if

$$\begin{cases}\widehat{\boldsymbol{X}}_i=\begin{bmatrix}\boldsymbol{X}_i&\boldsymbol{0}\\\boldsymbol{X}_{21i}&\boldsymbol{X}_{22i}\end{bmatrix}&(i=1,2,\ldots,N)\\\boldsymbol{X}_i=\boldsymbol{X}_i^{\mathrm{T}}>\boldsymbol{0}\end{cases} \tag{23}$$

The time derivate of $V(\widehat{\boldsymbol{x}}(t))$ along trajectories of the descriptor system Eq. (18) renders

$$\dot{\boldsymbol{V}}\left(\widehat{\boldsymbol{x}}(t)\right)+\widehat{\boldsymbol{x}}^{\mathrm{T}}(t)\,\widehat{\boldsymbol{Q}}\,\widehat{\boldsymbol{x}}(t)-\gamma^2\boldsymbol{r}^{\mathrm{T}}(t)\boldsymbol{r}(t)=\left[\widehat{\boldsymbol{x}}^{\mathrm{T}}(t),\boldsymbol{r}^{\mathrm{T}}(t)\right]\boldsymbol{\Omega}\left[\widehat{\boldsymbol{x}}^{\mathrm{T}}(t),\boldsymbol{r}^{\mathrm{T}}(t)\right]^{\mathrm{T}} \tag{24}$$

where

$$\begin{cases}\boldsymbol{\Omega}=\begin{bmatrix}\widehat{\boldsymbol{A}}_{\mathrm{h}}^{\mathrm{T}}\widehat{\boldsymbol{P}}_{\mathrm{v}}+\widehat{\boldsymbol{P}}_{\mathrm{v}}^{\mathrm{T}}\widehat{\boldsymbol{A}}_{\mathrm{h}}+\widehat{\boldsymbol{E}}^{\mathrm{T}}\dot{\widehat{\boldsymbol{P}}}_{\mathrm{v}}+\widehat{\boldsymbol{Q}} & * \\ \widehat{\boldsymbol{G}}^{\mathrm{T}}\widehat{\boldsymbol{P}}_{\mathrm{v}} & -\chi^2\boldsymbol{I}_{\bar{m}}\end{bmatrix}\\ \widehat{\boldsymbol{Q}}=\mathrm{diag}(\boldsymbol{Q},\boldsymbol{R})\end{cases}$$

with $\widehat{\boldsymbol{A}}_{\mathrm{h}}=\sum_{i=1}^{N}\mu_i\widehat{\boldsymbol{A}}_i$.

Multiplying $\boldsymbol{\Omega}$ on the left and right by $\mathrm{diag}(\widehat{\boldsymbol{X}}_{\mathrm{v}}^{\mathrm{T}},\boldsymbol{I}_{\bar{m}})$ and $\mathrm{diag}(\widehat{\boldsymbol{X}}_{\mathrm{v}},\boldsymbol{I}_{\bar{m}})$, respectively, we get a similar matrix $\widetilde{\boldsymbol{\Omega}}$. The property of μ_i defined by Eq. (5) and $\boldsymbol{X}_N-\boldsymbol{X}_i>\boldsymbol{0}$ ($i=1,2,\ldots,N-1$) yield

$$\begin{aligned}\widetilde{\boldsymbol{\Omega}}&=\begin{bmatrix}\boldsymbol{\Gamma}_{\mathrm{hv}}+\widehat{\boldsymbol{X}}_{\mathrm{v}}^{\mathrm{T}}\widehat{\boldsymbol{E}}^{\mathrm{T}}\dot{\widehat{\boldsymbol{P}}}_{\mathrm{v}}\widehat{\boldsymbol{X}}_{\mathrm{v}}+\widehat{\boldsymbol{X}}_{\mathrm{v}}^{\mathrm{T}}\widehat{\boldsymbol{Q}}\widehat{\boldsymbol{X}}_{\mathrm{v}} & * \\ \widehat{\boldsymbol{G}}^{\mathrm{T}} & -\chi^2\boldsymbol{I}_{\bar{m}}\end{bmatrix}\leqslant\bar{\boldsymbol{\Omega}}\\ &=\begin{bmatrix}\boldsymbol{\Gamma}_{\mathrm{hv}}+\boldsymbol{Z}+\widehat{\boldsymbol{X}}_{\mathrm{v}}^{\mathrm{T}}\widehat{\boldsymbol{Q}}\widehat{\boldsymbol{X}}_{\mathrm{v}} & * \\ \widehat{\boldsymbol{G}}^{\mathrm{T}} & -\chi^2\boldsymbol{I}_{\bar{m}}\end{bmatrix}\end{aligned} \tag{25}$$

with

$$\begin{cases}\boldsymbol{\Gamma}_{\mathrm{hv}}=\begin{bmatrix}\left(\begin{matrix}\boldsymbol{X}_{\mathrm{v}}^{\mathrm{T}}\overline{\boldsymbol{A}}_{\mathrm{h}}^{\mathrm{T}}+\boldsymbol{X}_{21\mathrm{v}}^{\mathrm{T}}\overline{\boldsymbol{B}}_{\mathrm{h}}^{\mathrm{T}}+\\ \overline{\boldsymbol{A}}_{\mathrm{h}}\boldsymbol{X}_{\mathrm{v}}+\overline{\boldsymbol{B}}_{\mathrm{h}}\boldsymbol{X}_{21\mathrm{v}}\end{matrix}\right) & * \\ \boldsymbol{X}_{22\mathrm{v}}^{\mathrm{T}}\overline{\boldsymbol{B}}_{\mathrm{h}}^{\mathrm{T}}-\boldsymbol{N}_{\mathrm{h}}+\boldsymbol{X}_{21\mathrm{v}} & \boldsymbol{X}_{22\mathrm{v}}^{\mathrm{T}}+\boldsymbol{X}_{22\mathrm{v}}\end{bmatrix}\\ \boldsymbol{Z}=\begin{bmatrix}\sum_{\hbar=1}^{N-1}\phi_{\hbar}(\boldsymbol{X}_N-\boldsymbol{X}_{\hbar}) & \boldsymbol{0}\\ \boldsymbol{0} & \boldsymbol{0}\end{bmatrix}\end{cases}$$

and $\overline{\boldsymbol{A}}_{\mathrm{h}}=\sum_{i=1}^{N}\mu_i\overline{\boldsymbol{A}}_i$, $\overline{\boldsymbol{B}}_{\mathrm{h}}=\sum_{i=1}^{N}\mu_i\overline{\boldsymbol{B}}_i$, $\boldsymbol{N}_{\mathrm{h}}=\sum_{i=1}^{N}\mu_i\boldsymbol{N}_i$, $\boldsymbol{X}_{\mathrm{v}}=\sum_{j=1}^{N}\mu_j\boldsymbol{X}_j$, $\boldsymbol{X}_{21\mathrm{v}}=\sum_{j=1}^{N}\mu_j\boldsymbol{X}_{21j}$, $\boldsymbol{X}_{22\mathrm{v}}=\sum_{j=1}^{N}\mu_j\boldsymbol{X}_{22j}$.

By Schur complement, LMI constraint of Eq. (19) renders $\bar{\boldsymbol{\Omega}}\leqslant\boldsymbol{0}$.[15,29] Then $\boldsymbol{\Omega}\leqslant\boldsymbol{0}$ and

$$\dot{\boldsymbol{V}}\left(\widehat{\boldsymbol{x}}(t)\right)+\widehat{\boldsymbol{x}}^{\mathrm{T}}(t)\,\widehat{\boldsymbol{Q}}\,\widehat{\boldsymbol{x}}(t)-\chi^2\boldsymbol{r}^{\mathrm{T}}(t)\boldsymbol{r}(t)\leqslant\boldsymbol{0} \tag{26}$$

The integral of Eq. (26) from $t=0$ to $t=T_{\mathrm{f}}$ yields $J\leqslant\bar{J}$, and this completes the proof.[30] □

Under the LMI constraint of Eq. (19), the system described by Eq. (17) leads to the reference closed-loop system

$$\dot{\bar{\boldsymbol{x}}}_{\mathrm{m}}(t)=\underbrace{\sum_{i=1}^{N}\mu_i\left(\overline{\boldsymbol{A}}_i+\overline{\boldsymbol{B}}_i\sum_{j=1}^{N}\mu_j\overline{\boldsymbol{K}}_j\right)}_{\overline{\boldsymbol{A}}_{\mathrm{mh}}}\bar{\boldsymbol{x}}_{\mathrm{m}}(t)+\overline{\boldsymbol{G}}\boldsymbol{r}(t) \tag{27}$$

where $\bar{\boldsymbol{x}}_{\mathrm{m}}(t)$ is the reference state and $\overline{\boldsymbol{A}}_{\mathrm{mh}}$ is the time-varying Hurwitz matrix for any $\boldsymbol{z}(t)\in\boldsymbol{\Omega}_{\boldsymbol{z}}$, which specifies the satisfactory tracking performances of the desirable commands $\boldsymbol{y}_{\mathrm{c}}(t)$.

Remark 1. The LMI constraint Eq. (19) degrades to a common Lyapunov function based constraint[15] if we set $\widehat{\boldsymbol{X}}_i=\widehat{\boldsymbol{X}}_j$ for any $i,j\in\{1,2,\ldots,N\}$ and $i\neq j$. Hence, the fuzzy baseline controller reduces the conservatism. Compared with Ref.[19], the computational complexity is reduced from $O(N^3)$ to $O(N^2)$. Where the function $O(\cdot)$ represents the computational complexity with respect to the number of fuzzy rules.

Remark 2. The control parameter can be optimized through adjusting $\boldsymbol{Q}$, $\boldsymbol{R}$ and the minimum χ constantly by adopting the function mincx(·) under the MATLAB LMI toolbox.[31]

3.2. Adaptive increment and stability analysis

Substituting the controller $\boldsymbol{u}(t)$ with $\boldsymbol{u}_{\mathrm{L}}(t)$ restricted by Eq. (19), we get an uncertain closed-loop system

$$\begin{aligned}\dot{\bar{\boldsymbol{x}}}(t)=\overline{\boldsymbol{A}}_{\mathrm{mh}}\bar{\boldsymbol{x}}(t)+\overline{\boldsymbol{B}}_{\mathrm{h}}\big[&\left(\boldsymbol{I}_{\bar{m}}+\boldsymbol{\Lambda}^{\mathrm{T}}(t)\right)\boldsymbol{u}_{\mathrm{A}}(t)+\boldsymbol{W}^{\mathrm{T}}\boldsymbol{\sigma}\left(\boldsymbol{V}^{\mathrm{T}}(t)\boldsymbol{\psi}(t)\right)\\&+\boldsymbol{\Lambda}^{\mathrm{T}}(t)\boldsymbol{u}_{\mathrm{L}}(t)+\boldsymbol{\varepsilon}(\boldsymbol{\psi}(t))\big]+\overline{\boldsymbol{G}}\boldsymbol{r}(t)\end{aligned} \tag{28}$$

Define the fuzzy premise variables based state predictor (the reference closed-loop system) as

$$\begin{aligned}\dot{\hat{\boldsymbol{x}}}(t)=\overline{\boldsymbol{A}}_{\mathrm{mh}}\hat{\boldsymbol{x}}(t)+\overline{\boldsymbol{B}}_{\mathrm{h}}\Big[&\left(\boldsymbol{I}_{\bar{m}}+\hat{\boldsymbol{\Lambda}}^{\mathrm{T}}(t)\right)\boldsymbol{u}_{\mathrm{A}}(t)+\hat{\boldsymbol{W}}^{\mathrm{T}}(t)\boldsymbol{\sigma}\left(\hat{\boldsymbol{V}}^{\mathrm{T}}(t)\boldsymbol{\psi}(t)\right)\\&+\hat{\boldsymbol{\Lambda}}^{\mathrm{T}}(t)\boldsymbol{u}_{\mathrm{L}}(t)\Big]+\overline{\boldsymbol{G}}\boldsymbol{r}(t)\end{aligned} \tag{29}$$

with $\hat{\boldsymbol{x}}(t)$ the predictor state, $\hat{\boldsymbol{W}}(t)$, $\hat{\boldsymbol{V}}(t)$ and $\hat{\boldsymbol{\Lambda}}(t)$ the adaptive parametric estimates of $\boldsymbol{W}$, $\boldsymbol{V}$ and $\boldsymbol{\Lambda}$.

Let the adaptive increment $\boldsymbol{u}_{\mathrm{A}}(t)$ be given by

$$\begin{aligned}\boldsymbol{u}_{\mathrm{A}}(t)=&-\left(\boldsymbol{I}_{\bar{m}}+\hat{\boldsymbol{\Lambda}}^{\mathrm{T}}(t)\right)^{-1}\\&\times\left[\hat{\boldsymbol{W}}^{\mathrm{T}}(t)\boldsymbol{\sigma}\left(\hat{\boldsymbol{V}}^{\mathrm{T}}(t)\boldsymbol{\psi}(t)\right)+\hat{\boldsymbol{\Lambda}}^{\mathrm{T}}(t)\boldsymbol{u}_{\mathrm{L}}(t)\right]\end{aligned} \tag{30}$$

and the existence of $\left(\boldsymbol{I}_{\bar{m}}+\hat{\boldsymbol{\Lambda}}^{\mathrm{T}}(t)\right)^{-1}$ will be addressed latter. By subtracting Eq. (28) from Eq. (29) and using Tayor series expansion of SHLNN about $(\boldsymbol{W}(t),\boldsymbol{V}(t))$, we can obtain the predication error system

$$\begin{aligned}\dot{\tilde{\boldsymbol{x}}}(t)=\overline{\boldsymbol{A}}_{\mathrm{mh}}\tilde{\boldsymbol{x}}(t)+\overline{\boldsymbol{B}}_{\mathrm{h}}\Big[&\widetilde{\boldsymbol{W}}^{\mathrm{T}}(t)\upsilon\left(\hat{\boldsymbol{V}}(t),\boldsymbol{\psi}(t)\right)\\&+\hat{\boldsymbol{W}}(t)^{\mathrm{T}}\nabla\boldsymbol{\sigma}\left(\hat{\boldsymbol{V}}(t)\boldsymbol{\psi}(t)\right)\tilde{\boldsymbol{V}}^{\mathrm{T}}(t)\boldsymbol{\psi}(t)+\tilde{\boldsymbol{\Lambda}}^{\mathrm{T}}(t)\boldsymbol{u}(t)\\&+\boldsymbol{\varsigma}(t)-\boldsymbol{\varepsilon}(\boldsymbol{\psi}(t))\Big]\end{aligned} \tag{31}$$

where $\tilde{\boldsymbol{x}}(t)=\hat{\boldsymbol{x}}(t)-\bar{\boldsymbol{x}}(t)$ is the predication error; $\widetilde{\boldsymbol{W}}(t)=\hat{\boldsymbol{W}}(t)-\boldsymbol{W}$, $\tilde{\boldsymbol{V}}(t)=\hat{\boldsymbol{V}}(t)-\boldsymbol{V}$ and $\tilde{\boldsymbol{\Lambda}}(t)=\hat{\boldsymbol{\Lambda}}(t)-\boldsymbol{\Lambda}$ are estimation errors of unknown $\boldsymbol{W}$, $\boldsymbol{V}$ and $\boldsymbol{\Lambda}$, and

$$\begin{cases}\upsilon\left(\hat{\boldsymbol{V}}(t),\boldsymbol{\psi}(t)\right)=\boldsymbol{\sigma}\left(\hat{\boldsymbol{V}}^{\mathrm{T}}(t)\boldsymbol{\psi}(t)\right)\\ \qquad-\nabla\boldsymbol{\sigma}\left(\hat{\boldsymbol{V}}^{\mathrm{T}}(t)\boldsymbol{\psi}(t)\right)\hat{\boldsymbol{V}}^{\mathrm{T}}(t)\boldsymbol{\psi}(t)\\ \boldsymbol{\varsigma}(t)=\widetilde{\boldsymbol{W}}^{\mathrm{T}}(t)\nabla\boldsymbol{\sigma}\left(\hat{\boldsymbol{V}}^{\mathrm{T}}(t)\boldsymbol{\psi}(t)\right)\boldsymbol{V}^{\mathrm{T}}\boldsymbol{\psi}(t)\\ \qquad+\boldsymbol{W}^{\mathrm{T}}\ell\left(\left\|\tilde{\boldsymbol{V}}^{\mathrm{T}}(t)\boldsymbol{\psi}(t)\right\|_{\mathrm{F}}^2\right)\end{cases} \tag{32}$$

with $\|\cdot\|_{\mathrm{F}}$ the Frobenius norm of the matrix. And $\ell\left(\left\|\tilde{\boldsymbol{V}}^{\mathrm{T}}(t)\boldsymbol{\psi}(t)\right\|_{\mathrm{F}}^2\right)$ represents the 2nd and higher order terms of the Taylor-series expansion, and $\left\|\tilde{\boldsymbol{V}}^{\mathrm{T}}(t)\boldsymbol{\psi}(t)\right\|_{\mathrm{F}}^2$ and $\ell\left(\left\|\tilde{\boldsymbol{V}}^{\mathrm{T}}(t)\boldsymbol{\psi}(t)\right\|_{\mathrm{F}}^2\right)\to0$ as $\left\|\tilde{\boldsymbol{V}}^{\mathrm{T}}(t)\boldsymbol{\psi}(t)\right\|_{\mathrm{F}}\to0$. $\nabla\boldsymbol{\sigma}(\hat{\boldsymbol{V}}^{\mathrm{T}}(t)\boldsymbol{\psi}(t))\in\mathbf{R}^{(l+1)\times l}$ is the Jacobian matrix as follows

$$\begin{aligned}&\nabla\boldsymbol{\sigma}\left(\hat{\boldsymbol{V}}^{\mathrm{T}}(t)\boldsymbol{\psi}(t)\right)\\&=\frac{\partial\boldsymbol{\sigma}\left(\hat{\boldsymbol{V}}^{\mathrm{T}}(t)\boldsymbol{\psi}(t)\right)}{\partial\hat{\boldsymbol{V}}^{\mathrm{T}}(t)\boldsymbol{\psi}(t)}\\&=\begin{bmatrix}0&0&0&0\\\frac{\partial\sigma_1(\rho_1)}{\partial\rho_1}&0&0&0\\0&\frac{\partial\sigma_2(\rho_2)}{\partial\rho_2}&\cdots&0\\\vdots&\vdots&\ddots&\vdots\\0&0&0&\frac{\partial\sigma_l(\rho_l)}{\partial\rho_l}\end{bmatrix}\end{aligned}\tag{33}$$

where $\rho_i=\hat{\boldsymbol{v}}_i^{\mathrm{T}}(t)\boldsymbol{\psi}(t)$ with $\hat{\boldsymbol{v}}_i$ the estimate of $\boldsymbol{v}_i$ and $\partial\sigma_i(\rho_i)/\partial\rho_i=\ a_i\mathrm{e}^{-a_i\rho_i}/(1+\mathrm{e}^{-a_i\rho_i})^2$, for any $i\in(1,2,\ldots,l)$.

The predication error system of Eq. (31) can be represented in terms of descriptor system

$$\begin{aligned}\widehat{\boldsymbol{E}}\dot{\breve{\boldsymbol{x}}}(t)=&\sum_{i=1}^{N}\mu_i\widehat{\boldsymbol{A}}_i(t)\breve{\boldsymbol{x}}(t)+\sum_{i=1}^{N}\mu_i\widehat{\boldsymbol{B}}_i(t)\\&\times\left[\widetilde{\boldsymbol{W}}^{\mathrm{T}}(t)\boldsymbol{\upsilon}\left(\hat{\boldsymbol{V}}(t),\boldsymbol{\psi}(t)\right)+\hat{\boldsymbol{W}}^{\mathrm{T}}(t)\right.\\&\times\nabla\boldsymbol{\sigma}\left(\hat{\boldsymbol{V}}^{\mathrm{T}}(t)\boldsymbol{\psi}(t)\right)\tilde{\boldsymbol{V}}^{\mathrm{T}}(t)\boldsymbol{\psi}(t)+\tilde{\boldsymbol{\Lambda}}^{\mathrm{T}}(t)\boldsymbol{u}(t)\\&\left.+\boldsymbol{\varsigma}(t)-\boldsymbol{\varepsilon}(\boldsymbol{\psi}(t))\right]\end{aligned}\tag{34}$$

with $\breve{\boldsymbol{x}}(t)=\left[\tilde{\boldsymbol{x}}^{\mathrm{T}}(t),\ \breve{\boldsymbol{u}}^{\mathrm{T}}(t)\right]^{\mathrm{T}},\widehat{\boldsymbol{B}}_i(t)=\left[\overline{\boldsymbol{B}}_i^{\mathrm{T}}(t),\boldsymbol{0}\right]^{\mathrm{T}}$ for $i=1,2,\ldots,N$, and $\breve{\boldsymbol{u}}(t)=-\sum_{i=1}^{N}\mu_i\overline{\boldsymbol{K}}_i\tilde{\boldsymbol{x}}(t)$.

Theorem 2. *Consider the uncertain fuzzy T–S system* Eq. (4) *with* $\boldsymbol{u}(t)$ *given by* Eq. (14), $\boldsymbol{u}_{\mathrm{L}}(t)$ *given by* Eq. (16) *satisfying LMI constraint* Eq. (19), $\boldsymbol{u}_{\Lambda}(t)$ *given by* Eq. (30), *the state predictor and predication error system given by* Eqs. (29) and (31) *with* $\hat{\boldsymbol{W}}(t)$, $\hat{\boldsymbol{V}}(t)$ *and* $\hat{\boldsymbol{\Lambda}}(t)$ *governed by projection-based*[4] *adaptation laws*

$$\begin{cases}\dot{\hat{\boldsymbol{W}}}(t)=\boldsymbol{\Gamma}\ \mathrm{Proj}\left(\hat{\boldsymbol{W}}(t),-\boldsymbol{\upsilon}\left(\hat{\boldsymbol{V}}(t),\boldsymbol{\psi}(t)\right)\boldsymbol{\xi}(t)\right)\\\dot{\hat{\boldsymbol{V}}}(t)=\boldsymbol{F}\ \mathrm{Proj}\left(\hat{\boldsymbol{V}}(t),-\boldsymbol{\psi}(t)\boldsymbol{\xi}(t)\hat{\boldsymbol{W}}^{\mathrm{T}}\nabla\boldsymbol{\sigma}\left(\hat{\boldsymbol{V}}^{\mathrm{T}}(t)\boldsymbol{\psi}(t)\right)\right)\\\dot{\hat{\boldsymbol{\Lambda}}}(t)=\boldsymbol{T}\ \mathrm{Proj}\left(\hat{\boldsymbol{\Lambda}}(t),-\boldsymbol{u}(t)\boldsymbol{\xi}(t)\right)\end{cases}\tag{35}$$

where the filtered prediction error is

$$\boldsymbol{\xi}(t)=\tilde{\boldsymbol{x}}^{\mathrm{T}}(t)\bar{\boldsymbol{P}}_{\mathrm{v}}\overline{\boldsymbol{B}}_{\mathrm{h}}\tag{36}$$

with

$$\bar{\boldsymbol{P}}_{\mathrm{v}}=\left[\boldsymbol{I}_{\bar{n}\times\bar{n}}^{\mathrm{T}},\boldsymbol{0}_{\bar{m}\times\bar{n}}^{\mathrm{T}}\right]\left(\sum_{j=1}^{N}\mu_j\widehat{\boldsymbol{X}}_j\right)^{-1}\begin{bmatrix}\boldsymbol{I}_{\bar{n}\times\bar{n}}^{\mathrm{T}}\\\boldsymbol{0}_{\bar{m}\times\bar{n}}^{\mathrm{T}}\end{bmatrix}\tag{37}$$

and the adaptation rates $\boldsymbol{\Gamma}\in\mathbf{R}^{(l+1)\times(l+1)}$, $\boldsymbol{T}\in\mathbf{R}^{\bar{m}\times\bar{m}}$, *and* $\boldsymbol{F}\in\mathbf{R}^{(n+K+1)\times(n+K+1)}$ *are diagonal positive define matrices. Then,* $(\tilde{\boldsymbol{x}}(t),\widetilde{\boldsymbol{W}}(t),\tilde{\boldsymbol{V}}(t),\tilde{\boldsymbol{\Lambda}}(t))$ *of the predication error system* (31) *is uniformly ultimately bounded* (*UUB*) *for any* $(\boldsymbol{x}(t),\boldsymbol{z}(t))\in\boldsymbol{\Omega}_x\times\boldsymbol{\Omega}_z$ *with an ultimate bound* $\|\tilde{\boldsymbol{x}}(t)\|\leqslant\tilde{x}_{\mathrm{b}}$,

$$\tilde{x}_{\mathrm{b}}=\sqrt{\frac{\left(\sqrt{\rho_0^2+\rho_1}+\rho_0\right)^2+\rho_2}{\lambda_{z\min}\left(\bar{\boldsymbol{P}}_{\mathrm{v}}\right)}}\tag{38}$$

with

$$\begin{cases}\rho_0=\dfrac{\lambda_{z\max}\left(\bar{\boldsymbol{P}}_{\mathrm{v}}\right)\bar{b}(\bar{\varepsilon}+\bar{\varsigma})}{\lambda_{\min}(\boldsymbol{Q})}\\\rho_1=\dfrac{4\bar{\Gamma}\bar{d}_{\Gamma}}{\lambda_{\min}(\boldsymbol{T})\lambda_{\min}(\boldsymbol{Q})}\\\rho_2=\dfrac{4\bar{W}^2}{\lambda_{\min}(\boldsymbol{\Gamma})}+\dfrac{4\bar{V}^2}{\lambda_{\min}(\boldsymbol{F})}+\dfrac{4\bar{\Gamma}^2}{\lambda_{\min}(\boldsymbol{T})}\end{cases}\tag{39}$$

where $\lambda_{\min}(\cdot)$, $\lambda_{\max}(\cdot)$ *are the minimum and maximum eigenvalues of the matrices;* $\bar{\varsigma}>0$ *is a constant, with* $\|\boldsymbol{\varsigma}(t)\|\leqslant\bar{\varsigma}$ *satisfied; and*

$$\begin{cases}\lambda_{z\max}(\cdot)=\sup\limits_{\boldsymbol{z}(t)\in\boldsymbol{\Omega}_z}\lambda_{\max}(\cdot)\\\lambda_{z\min}(\cdot)=\inf\limits_{\boldsymbol{z}(t)\in\boldsymbol{\Omega}_z}\lambda_{\min}(\cdot)\\\bar{b}=\max\limits_{\boldsymbol{z}(t)\in\boldsymbol{\Omega}_z}\left\|\overline{\boldsymbol{B}}_{\mathrm{h}}\right\|_{\mathrm{F}}\\\bar{W}=\sum\limits_{i=1}^{l}\bar{w}_i,\ \bar{V}=\sum\limits_{i=1}^{\bar{m}}\bar{v}_i\\\bar{\Gamma}=\sum\limits_{i=1}^{\bar{m}}\bar{\Lambda}_i,\bar{d}_{\Gamma}=\sum\limits_{i=1}^{\bar{m}}\bar{d}_{\Lambda i}\end{cases}$$

Hence, the controller guarantees a UUB close-loop system under undesirable uncertainties, and it constitutes the fuzzy adaptive tracking controller within the full envelope for the UAV as shown in Fig. 2.

Proof. Consider the following candidate fuzzy multiple Lyapunov-like function

$$\begin{aligned}\boldsymbol{V}\left(\breve{\boldsymbol{x}}(t)\right)=&\breve{\boldsymbol{x}}^{\mathrm{T}}(t)\widehat{\boldsymbol{E}}^{\mathrm{T}}\widehat{\boldsymbol{P}}_{\mathrm{v}}\breve{\boldsymbol{x}}(t)+\mathrm{tr}\left(\widetilde{\boldsymbol{W}}^{\mathrm{T}}(t)\boldsymbol{\Gamma}^{-1}\widetilde{\boldsymbol{W}}^{\mathrm{T}}(t)\right)\\&+\mathrm{tr}\left(\tilde{\boldsymbol{V}}^{\mathrm{T}}(t)\boldsymbol{F}^{-1}\tilde{\boldsymbol{V}}(t)\right)+\mathrm{tr}\left(\tilde{\boldsymbol{\Lambda}}^{\mathrm{T}}(t)\boldsymbol{T}^{-1}\tilde{\boldsymbol{\Lambda}}(t)\right)\end{aligned}\tag{40}$$

with $\widehat{\boldsymbol{P}}_{\mathrm{v}}$ restrained by Eq. (22) and $\mathrm{tr}(\cdot)$ the trace operator. The time derivate of $\boldsymbol{V}(\breve{\boldsymbol{x}}(t))$ can be written as

$$\begin{aligned}\dot{\boldsymbol{V}}\left(\breve{\boldsymbol{x}}(t)\right)=&\breve{\boldsymbol{x}}^{\mathrm{T}}(t)\left(\widehat{\boldsymbol{A}}_{\mathrm{h}}^{\mathrm{T}}\widehat{\boldsymbol{P}}_{\mathrm{v}}+\widehat{\boldsymbol{P}}_{\mathrm{v}}^{\mathrm{T}}\widehat{\boldsymbol{A}}_{\mathrm{h}}+\widehat{\boldsymbol{E}}^{\mathrm{T}}\dot{\widehat{\boldsymbol{P}}}_{\mathrm{v}}\right)\breve{\boldsymbol{x}}(t)\\&+2\breve{\boldsymbol{x}}^{\mathrm{T}}(t)\widehat{\boldsymbol{P}}_{\mathrm{v}}^{\mathrm{T}}\widehat{\boldsymbol{B}}_{\mathrm{h}}\left[\widetilde{\boldsymbol{W}}^{\mathrm{T}}\boldsymbol{\upsilon}\left(\hat{\boldsymbol{V}}(t),\boldsymbol{\psi}(t)\right)\right.\\&\left.+\hat{\boldsymbol{W}}^{\mathrm{T}}(t)\nabla\boldsymbol{\sigma}\left(\hat{\boldsymbol{V}}^{\mathrm{T}}(t)\boldsymbol{\psi}(t)\right)\tilde{\boldsymbol{V}}^{\mathrm{T}}(t)\boldsymbol{\psi}(t)+\tilde{\boldsymbol{\Lambda}}^{\mathrm{T}}(t)\boldsymbol{u}(t)\right.\\&\left.+\boldsymbol{\varsigma}(t)-\boldsymbol{\varepsilon}(\boldsymbol{\psi}(t))\right]+2\mathrm{tr}\left(\widetilde{\boldsymbol{W}}^{\mathrm{T}}(t)\boldsymbol{\Gamma}^{-1}\dot{\hat{\boldsymbol{W}}}(t)\right)\\&+2\mathrm{tr}\left(\tilde{\boldsymbol{V}}^{\mathrm{T}}(t)\boldsymbol{F}^{-1}\dot{\hat{\boldsymbol{V}}}(t)\right)+2\mathrm{tr}\left(\tilde{\boldsymbol{\Lambda}}^{\mathrm{T}}(t)\mathrm{T}^{-1}\dot{\hat{\boldsymbol{\Lambda}}}(t)\right)\\&-2\mathrm{tr}\left(\tilde{\boldsymbol{\Lambda}}^{\mathrm{T}}(t)\boldsymbol{T}^{-1}\dot{\boldsymbol{\Lambda}}(t)\right)\end{aligned}\tag{41}$$

with $\widehat{\boldsymbol{B}}_{\mathrm{h}}=\sum_{i=1}^{N}\mu_i\widehat{\boldsymbol{B}}_i$.

Since the LMI constraint of Eq. (19) guarantees $\boldsymbol{\Omega}\leqslant\boldsymbol{0}$ as defined in Eq. (24), with Schur complement, we can get

$$\breve{\boldsymbol{x}}^{\mathrm{T}}(t)\left(\widehat{\boldsymbol{A}}_{\mathrm{h}}^{\mathrm{T}}\widehat{\boldsymbol{P}}_{\mathrm{v}}+\widehat{\boldsymbol{P}}_{\mathrm{v}}^{\mathrm{T}}\widehat{\boldsymbol{A}}_{\mathrm{h}}+\widehat{\boldsymbol{E}}^{T}\dot{\widehat{\boldsymbol{P}}}_{\mathrm{v}}\right)\breve{\boldsymbol{x}}(t)\leqslant-\tilde{\boldsymbol{x}}^{\mathrm{T}}(t)\boldsymbol{Q}\tilde{\boldsymbol{x}}(t)\tag{42}$$

The constraint condition by Eq. (22) renders $\boldsymbol{\xi}(t)=\breve{\boldsymbol{x}}^{\mathrm{T}}(t)\widehat{\boldsymbol{P}}_{\mathrm{v}}^{\mathrm{T}}\widehat{\boldsymbol{B}}_{\mathrm{h}}=\tilde{\boldsymbol{x}}^{\mathrm{T}}(t)\bar{\boldsymbol{P}}_{\mathrm{v}}\overline{\boldsymbol{B}}_{\mathrm{h}}$. By Assumptions 1 and 2, we can obtain $\boldsymbol{W}\in\boldsymbol{\Omega}_W=\left\{\boldsymbol{W}\middle|\|\boldsymbol{W}\|_{\mathrm{F}}<\bar{W}\right\}$, $\boldsymbol{V}\in\boldsymbol{\Omega}_V=\left\{\boldsymbol{V}\middle|\|\boldsymbol{V}\|_{\mathrm{F}}<\bar{V}\right\},\boldsymbol{\Lambda}\in\boldsymbol{\Omega}_{\Lambda}=\left\{\boldsymbol{\Lambda}\middle|\|\boldsymbol{\Lambda}\|_{\mathrm{F}}<\bar{\Gamma}\right\}$. The projection operators in Eq. (35) ensure $\hat{\boldsymbol{W}}(t)\in\boldsymbol{\Omega}_W,\hat{\boldsymbol{V}}(t)\in\boldsymbol{\Omega}_V$ and $\hat{\boldsymbol{\Lambda}}(t)\in\boldsymbol{\Omega}_{\Lambda}$. Hence, the boundedness of $\widetilde{\boldsymbol{W}}(t),\tilde{\boldsymbol{V}}(t)$ and $\tilde{\boldsymbol{\Lambda}}(t)$ can be guaranteed and there exists a constant $\bar{\varsigma}>0$ so that $\|\boldsymbol{\varsigma}(t)\|\leqslant\bar{\varsigma}$. Using $\boldsymbol{a}^{\mathrm{T}}\boldsymbol{b}=\mathrm{tr}(\boldsymbol{b}\boldsymbol{a}^{\mathrm{T}})$, we get

$$\begin{aligned}\dot{\boldsymbol{V}}\left(\breve{\boldsymbol{x}}(t)\right)\leqslant&-\lambda_{\min}(\boldsymbol{Q})\|\tilde{\boldsymbol{x}}(t)\|^2+2\boldsymbol{\xi}(t)\times(\boldsymbol{\varsigma}(t)-\boldsymbol{\varepsilon}(\boldsymbol{\psi}(t)))\\&-2\mathrm{tr}\left(\tilde{\boldsymbol{\Lambda}}^{T}(t)\boldsymbol{T}^{-1}\dot{\boldsymbol{\Lambda}}(t)\right)\\\leqslant&\lambda_{\min}(\boldsymbol{Q})\left[-(\|\tilde{\boldsymbol{x}}(t)\|-\rho_0)^2+\rho_1+\rho_0^2\right]\end{aligned}\tag{43}$$

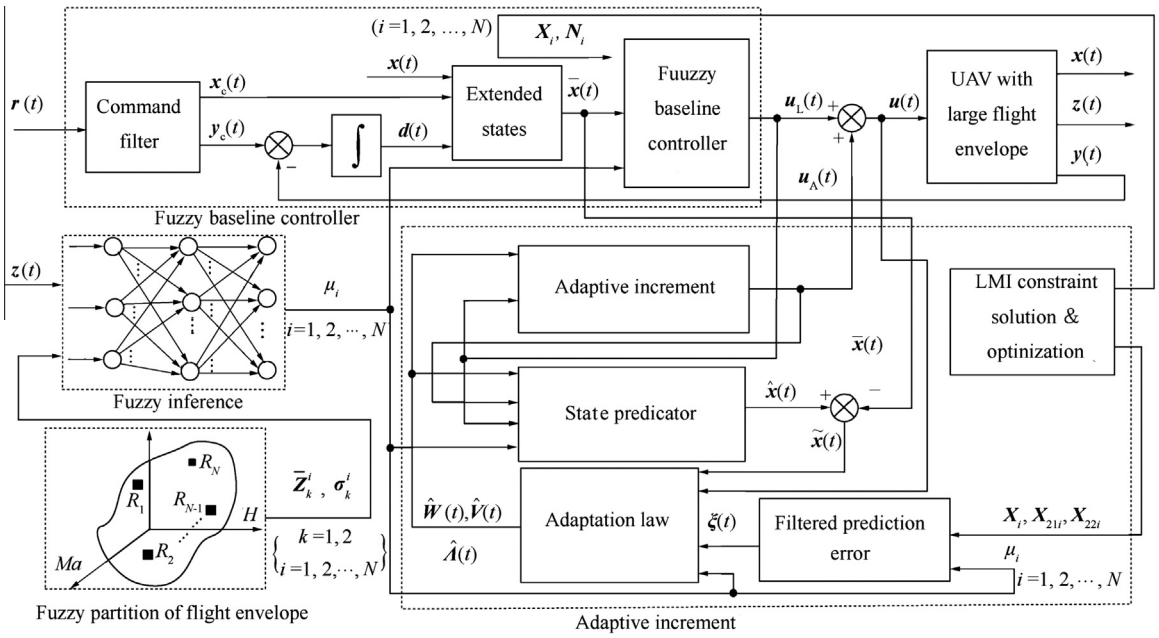

Fig. 2 Control architecture of fuzzy adaptive tracking controller.

Notice $\dot{V}(\tilde{\boldsymbol{x}}(t)) \leqslant 0$, if $\|\tilde{\boldsymbol{x}}(t)\| \geqslant \tilde{x}_{\max} = \sqrt{\rho_0^2 + \rho_1} + \rho_0$. Therefore, we can get

$$V_{\max} = \lambda_{z\max}(\bar{\boldsymbol{P}}_{\mathrm{v}})\tilde{x}_{\max}^2 + 4\bar{W}^2/\lambda_{\min}(\boldsymbol{\Gamma}) + 4\bar{V}^2/\lambda_{\min}(\boldsymbol{F}) + 4\bar{\Gamma}^2/\lambda_{\min}(\boldsymbol{T}) \tag{44}$$

Since $V(\tilde{\boldsymbol{x}}(0)) \leqslant V_{\max}$, we obtain $V(\tilde{\boldsymbol{x}}(t)) \leqslant V_{\max}$ and for all $t \geqslant 0$,

$$\lambda_{z\min}(\bar{\boldsymbol{P}}_{\mathrm{v}})\|\tilde{\boldsymbol{x}}(t)\|^2 \leqslant V_{\max} \tag{45}$$

which yields $\|\tilde{\boldsymbol{x}}(t)\| \leqslant \tilde{x}_{\mathrm{b}}$ and $\tilde{\boldsymbol{x}}(t), \widetilde{\boldsymbol{W}}(t), \tilde{\boldsymbol{V}}(t)$ and $\tilde{\boldsymbol{\Lambda}}(t)$ are UUB, which completes the proof. □

Remark 3. Notice that $\|\boldsymbol{\Lambda}(t)\|_{\mathrm{F}} < \bar{\Gamma} < 1$ renders $\lambda_{\max}(\hat{\boldsymbol{\Lambda}}(t)) < \bar{\Gamma}$. Hence, $(\boldsymbol{I}_{\bar{m}} + \hat{\boldsymbol{\Lambda}}^{\mathrm{T}}(t))^{-1}$ exists for any $t > 0$, which follows the fact that $\det(\boldsymbol{A} + \boldsymbol{B}) \neq 0$ if and only if there exists $\delta > 0$ so that $\lambda_{\min}(\boldsymbol{A}) > \delta$ and $\lambda_{\max}(\boldsymbol{B}) \leqslant \delta$, where $\det(\cdot)$ denotes the determinant of a matrix.

Remark 4. The state predictor of Eq. (29) with the adaptive increment of Eq. (30) is equivalent to the reference closed-loop system of Eq. (27). $\tilde{\boldsymbol{x}}(t)$ is UUB and it can be arbitrarily reduced via increasing $\boldsymbol{\Gamma}$, $\boldsymbol{F}$ and $\boldsymbol{T}$, which indicates the recovery of satisfactory tracking performances specified by the reference closed-loop system with strong robustness to uncertainties.

Remark 5. The fuzzy multiple Lyapunov function based adaptation laws improve the applicability of the adaptive increment for the compensation of uncertainties within the full envelope.

4. Simulations

In this section, we demonstrate the efficiency of the proposed controller under the nonlinear model of a prototype UAV. The flight envelope is restricted by the stall angle of attack 16°, the service ceiling 12 km, the maximum Mach number 1.4, and the maximum dynamic press 51.147 kPa. The saturation limits of δ_{th} and δ_{e} are set to (20%,100%) and (−25°, 25°), with the dynamics $5/(s + 5)$ and $15/(s + 15)$, respectively. The wing-plant and inertia parameters are shown in Table 1, while the aerodynamic derivatives under different Mach numbers are represented in Table 2. Following Ref.[26], we construct the fuzzy T–S model with $N = 11$ fuzzy rules.

Fig. 3 represents the fuzzy partition of the flight envelope with the brightness indicating the maximum membership degrees $\mu_{\max}(\boldsymbol{z}) = \max_{1\leqslant i\leqslant 11}(\mu_i)$ of the operating point to the 11 fuzzy rules. The fuzzy partition reflects composition results of 11 overlapped ellipses for the flight envelope region. We can find that it is bright to certain degree near the boundary of the flight envelope, so the universe of discourse for Gaussian membership functions of all the fuzzy rules exceeds the flight envelope boundary and covers the entire flight envelope region sufficiently.

Following the Theorem 1 and 2, we can construct the FATC for the prototype UAV. The command filter is defined as follows

$$\begin{cases} \boldsymbol{A}_{\mathrm{c}} = \begin{bmatrix} 0 & 1 & 0 & 0 \\ -0.533 & -1.285 & 0 & 0 \\ 0 & 0 & 0 & 1 \\ 0 & 0 & -0.423 & -1.14 \end{bmatrix} \\ \boldsymbol{B}_{\mathrm{c}} = \begin{bmatrix} 0 & 0 \\ 0.533 & 0 \\ 0 & 0 \\ 0 & 0.423 \end{bmatrix} \\ \boldsymbol{C}_{\mathrm{c}} = \begin{bmatrix} 1 & 0 & 0 & 0 \\ 0 & 0 & 1 & 0 \end{bmatrix} \end{cases}$$

Table 1 Wing-platform and inertia parameters.

Parameter	Value	Parameter	Value	Parameter	Value
m (kg)	12495	S(m^2)	39.5	x_{cgR}	0.33
J_z (kg · m^2)	23516	φ(°)	8	α(°)	−0.5
$\bar{c}$ (m)	6.3	e_{p}(m)	−0.6	b(m)	8.9

Table 2 Aerodynamic derivatives with respect to Mach number.

Mach number	Aerodynamic derivatives								
Ma	$C_{L\alpha}$	$C_{L\delta_e}$	C_{D0}	A	C_{M0}	C_{Mq}	$C_{M\delta_e}$	$C_{M\dot{\alpha}}$	x_{caR}
0.6	0.0481	0.0092	0.0182	0.2834	−0.0085	−1.5265	−0.0097	−0.6657	0.3853
0.7	0.0490	0.0094	0.0289	0.2845	−0.0088	−1.5600	−0.0097	−0.7164	0.3855
0.8	0.0504	0.0096	0.0338	0.2865	−0.0092	−1.6127	−0.0099	−0.7761	0.3904
0.9	0.0535	0.0097	0.0377	0.2896	−0.0105	−1.7533	−0.0102	−0.8912	0.3873
1.0	0.0546	0.0085	0.0405	0.3075	−0.0102	−2.0537	−0.0108	−0.9823	0.4342
1.1	0.0496	0.0066	0.0456	0.3595	−0.0051	−1.9732	−0.0092	−0.8767	0.4711
1.2	0.0472	0.0060	0.0387	0.3861	−0.0027	−2.0645	−0.0081	−0.7762	0.5012
1.3	0.0465	0.0057	0.0375	0.4274	−0.0014	−1.9577	−0.0070	−0.6190	0.5193
1.4	0.0457	0.0055	0.0342	0.4696	−0.0011	−1.8128	−0.0062	−0.5036	0.5163

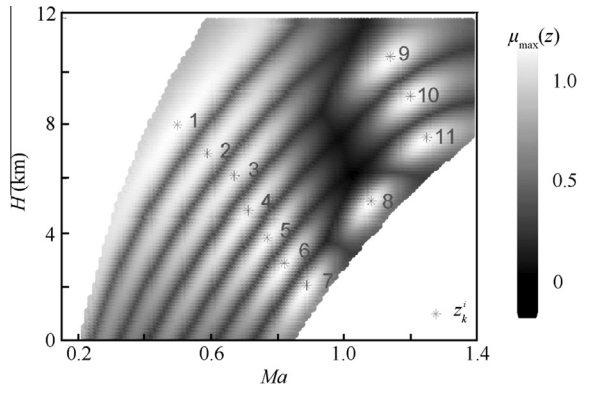

Fig. 3 Fuzzy partition of flight envelope.

Let $\boldsymbol{\beta} = [4.3, 4.6, 5.5, 6.7, 7.9, 9.1, 9.8, 9.2, 6.3]^{\mathrm{T}}$, we get $\chi^2 = 0.37$ with $\boldsymbol{Q} = \mathrm{diag}(10^{-4}\boldsymbol{I}_9, 1.2\boldsymbol{I}_2)$ and $\boldsymbol{R} = \mathrm{diag}(10^{-4}, 10^{-4})$ following Remark 2. Then, the control parameters $\boldsymbol{N}_i, \boldsymbol{X}_i, \boldsymbol{X}_{21i}$ and $\boldsymbol{X}_{22i}$ can be obtained ($i = 1, 2, \ldots, 11$), and we show $\boldsymbol{N}_i$ and $\boldsymbol{X}_1$, $\boldsymbol{X}_4$, $\boldsymbol{X}_{11}$ as examples in Appendix A. We design the SHLNN with 9 nodes in the input layer, 20 nodes in the hidden layer, and 2 nodes in the output layer. The parameters $a_i = 10^{(2(i-1)/19\ )-4}$ ($i = 1, 2, \ldots, 20$) cover the range between 0.0001 and 0.01, and $\boldsymbol{\Gamma} = 10\boldsymbol{I}_{21}$, $\boldsymbol{F} = 500\boldsymbol{I}_9$, $\boldsymbol{T} = 1.5\boldsymbol{I}_2$. The column norm bounds of adaptive parametric estimates $\hat{\boldsymbol{W}}(t)$, $\hat{\boldsymbol{V}}(t)$ and $\hat{\boldsymbol{\Lambda}}(t)$ are as $\bar{w}_i = 1.2$ ($i = 1, 2$), $\bar{\Lambda}_k = 0.4 (k = 1, 2)$, $\bar{v}_j = 1.0$ ($j = 1, 2, \ldots, 20$). According to Theorem 1, we can realize the controller $\boldsymbol{u}(t)$ given by Eq. (14), and $\boldsymbol{u}_{\mathrm{L}}(t)$ given by Eq. (16) satisfying LMI constraint of Eq. (19), $\boldsymbol{u}_{\mathrm{A}}(t)$ given by Eq. (30).

As the contrast of the FATC, a generalized fuzzy adaptive controller (GFAC) and a multi-model switching controller (MMSC) are constructed. The GFAC augments the common Lyapunov function based fuzzy baseline controller as Remark 1 with an L1 adaptive increment.[8,17] The MMSC divides the flight envelope into 3 locally overlapped subsystems: P1: 0 km $\leqslant H \leqslant$ 5.5 km; P2: 5 km $\leqslant H \leqslant$ 9 km; P3: 8.5 km $\leqslant H \leqslant$ 12 km. For any subsystem, $N = 6$ polytopic vertices are determined, and a local robust $H\infty$ LPV controller is designed by employing the common Lyapunov function and considering maximum uncertainties $\Delta\boldsymbol{A}_{si} = 0.15\boldsymbol{A}_{si}$, $\Delta\boldsymbol{B}_{si} = 0.15\boldsymbol{B}_{si}$ ($i = 1, 2, \ldots, 6; s = 1, 2, 3$) and $\boldsymbol{A}_{si}$ and $\boldsymbol{B}_{si}$ are the local system matrices of the ith fuzzy rule in the sth subsystem The local controllers switch using hysteretic switching logic.[10]

Under the nonlinear kinetic model of the UAV given by Eq. (1), the tracking performances of desirable commands are compared by employing the FATC, the GFAC, and the MMSC, respectively in the following sections. Two simulation cases are considered:

(1) Step responses at test operating points covering the entire envelope;
(2) A continuous flight over the large flight envelope span.

4.1. Tracking performances at the test points

As shown in Fig. 4, 58 test points are determined[1] to cover the entire flight envelope. We also select three navigation points (A, B and C) to identify the flight trajectory over the large

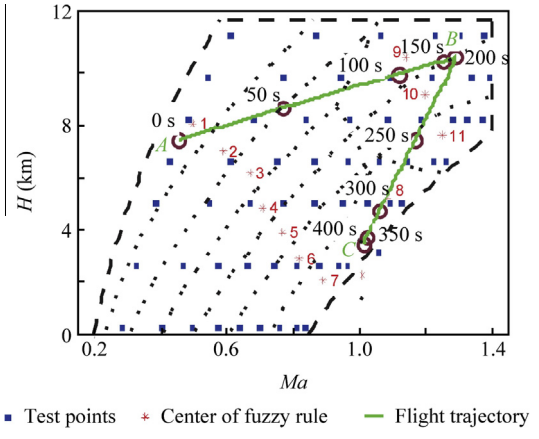

Fig. 4 Flight test points and flight trajectory over large envelope span.

Table 3 Parametric perturbations.

Parameter	Perturbation values (%)	Parameter	Perturbation values (%)
$C_{L\alpha}$	30	C_{Mq}	−30
$C_{L\delta_e}$	30	C_{M0}	−30
C_{D0}	−30	x_{cgR}	30
A	−30	X_{caR}	−30
$C_{m\delta_e}$	−30	T	−30

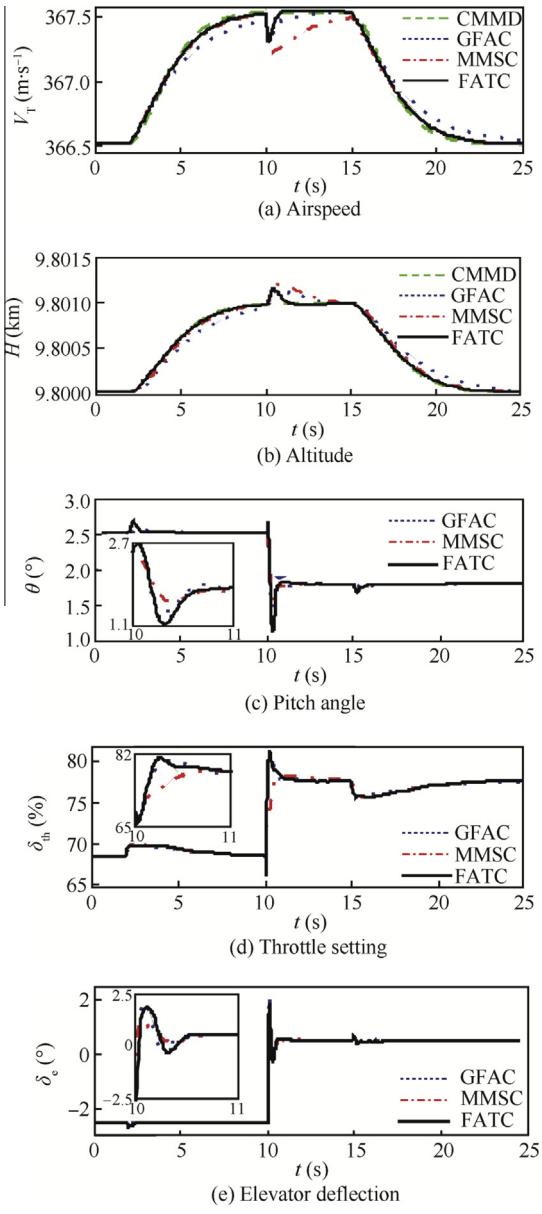

Fig. 5 Step response comparison at a specific test point with 3 controllers.

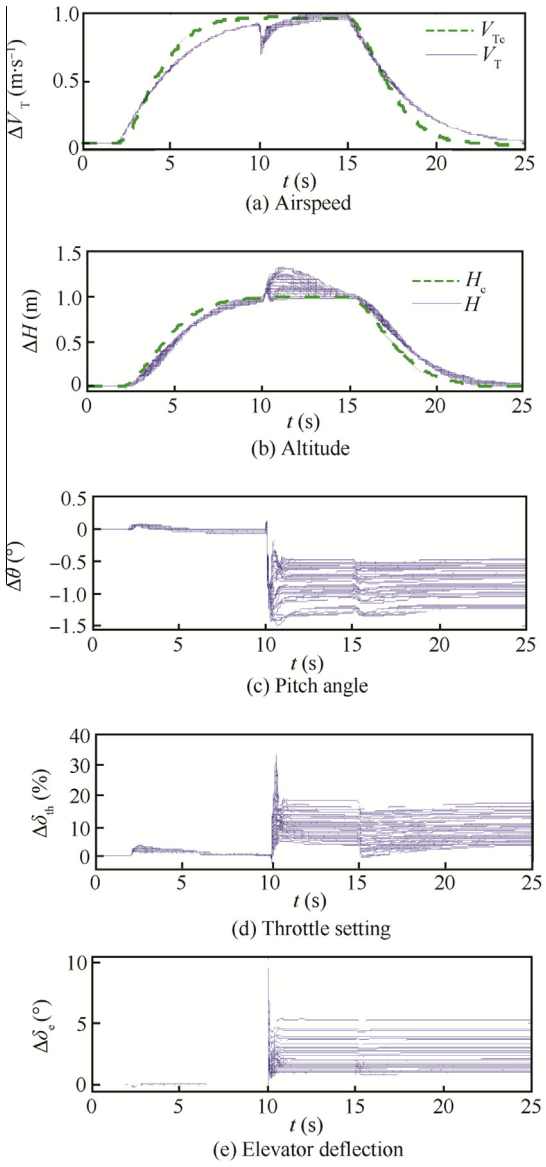

Fig. 6 Step responses of the closed-loop system with GFAC for all test points.

envelope span. To verify the robustness at the 58 test points, we conduct the large perturbations of aerodynamic parameters referring to the nominal values as shown in Table 3. The perturbations create bad conditions involving increased lift, reduced drag, control efficiency failures, and deterioration of airspeed static stability. For any test point, the simulation is initialized at the equilibrium state, and the rising step commands of airspeed and altitude are implemented at 2 s to illustrate the tracking performance in the absence of uncertainties between 2 s and 10 s. The perturbations are injected at 10 s, and the attenuation performance for instantly imposed uncertainties can be shown during (10 s, 15 s). The falling step commands are conducted at 15 s to illustrate the tracking performance in the presence of uncertainties between 15 s and 25 s.

As an illustration, the step responses at a specific test point (Ma = 1.22, H = 9.8 km) with the three controllers are represented in Fig. 5. Where CMMD represents the airspeed and altitude command in Fig. 5(a) and (b), respectively.

From Fig. 5, we can find that for the tracking responses of the step commands during the time intervals (2 s, 10 s) and (15 s, 25 s), the MMSC and the FATC both provide better tracking performances for the desirable airspeed and altitude commands (CMMD) on transient and steady-state than the GFAC. The GFAC degrades the tracking performance due to the conservatism for the entire flight envelope. After the exertion of uncertainties at 15 s, the MMSC just generates relatively smaller adjustments of throttle setting and elevator deflection with slower response rates and it leads to largest tracking errors and longest adjustment time. Hence, the local LPV robust controller attenuates the imposed uncertainties at the cost of response performances. Though the GFAC reduces the tracking errors obviously via the quick compensation of the L1 adaptive increment, the convergence time is

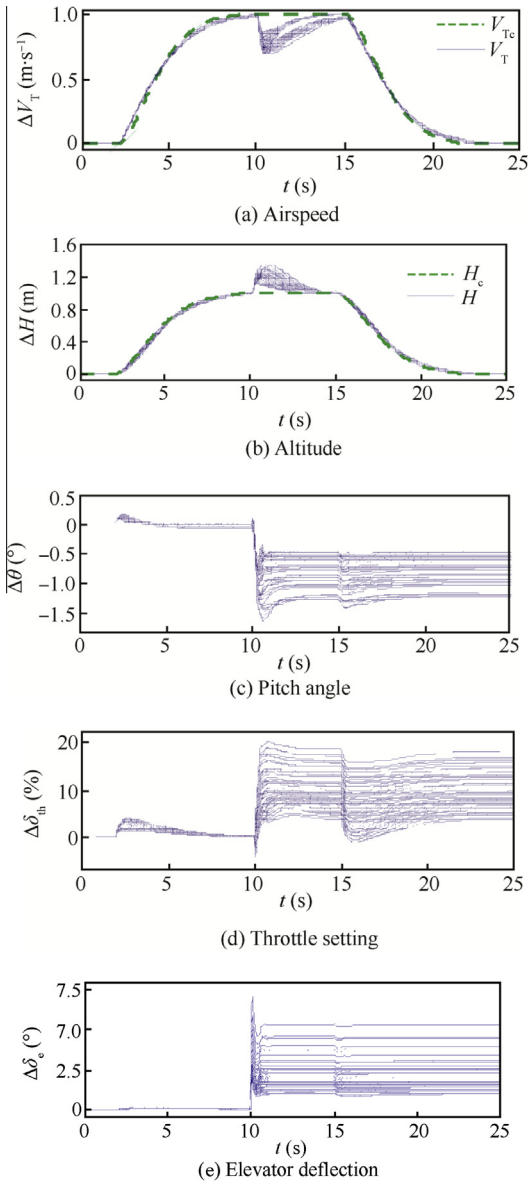

Fig. 7 Step responses of the closed-loop system with MMSC for all test points.

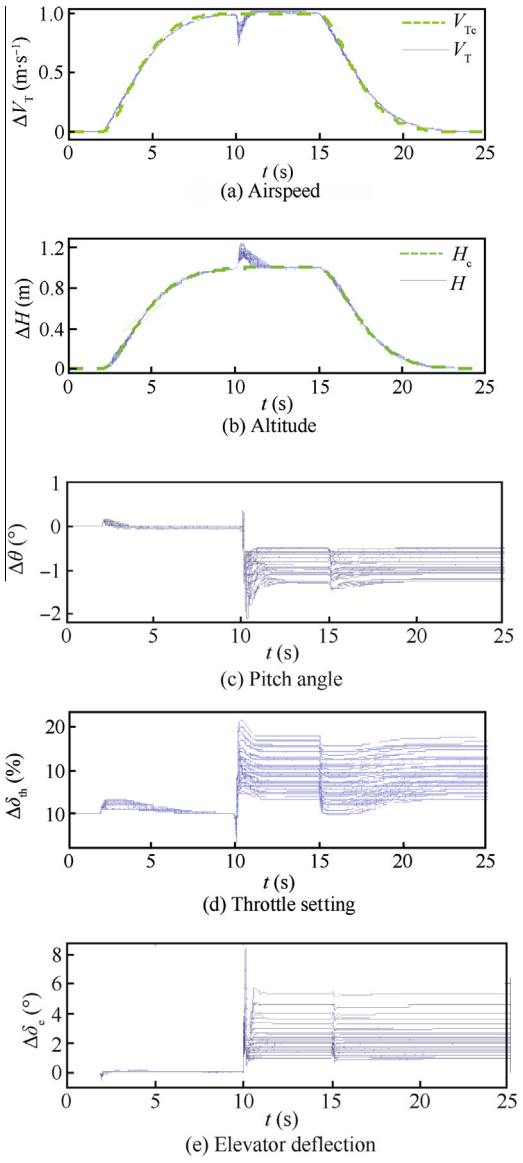

Fig. 8 Step responses of the closed-loop system with FATC for all test points.

longer than that of the FATC due to the poor responses of the fuzzy baseline controller. Benefiting from less conservatism and rapid compensation of the adaptive SHLNN increment without sacrificing the response quality, the FATC guarantees superior tracking performances with strong attenuation performances for the instantly imposed undesirable uncertainties. Hence, the proposed FATC improves response and robust performances simultaneously at the specific test point.

The responses of the closed-loop system with the three controllers for all the test points are represented in Figs. 6–8, respectively, in which symbol Δ denotes the deviation value of the signal with respect to the trimmed value at the corresponding point.

The statistic results of the tracking errors are represented in Figs. 9 and 10. Fig. 9 focuses on the step responses during the time intervals (2 s, 10 s) and (15 s, 25 s), and subscripts R and F label the rising step and the falling step, respectively. V_{Te}, H_e represent the maximum tracking errors of airspeed and altitude, while T_{eV}, T_{eH} indicate the response time errors at the corresponding test point. Fig. 10 shows the attenuation performances after the exertion of uncertainties between (10 s, 15 s), providing the maximum induced tracking errors V_{Te}, H_e and the required convergence times T_{eV}, T_{eH} to 10% of the maximum induced errors at the corresponding test point.

From Figs. 6–8, we get that though all the three controllers guarantee stable responses throughout the entire flight envelope, the tracking performances and uncertainties attenuation performances are different, and this can be concluded according to the statistic results in Figs. 9 and 10. For the tracking responses of rising and failing step commands, the GFAC leads to the largest tracking errors and response time errors obviously, though the SMMC improves the tracking performances and the responses within the whole envelope are more dispersed compared with those of the FATC. The FATC

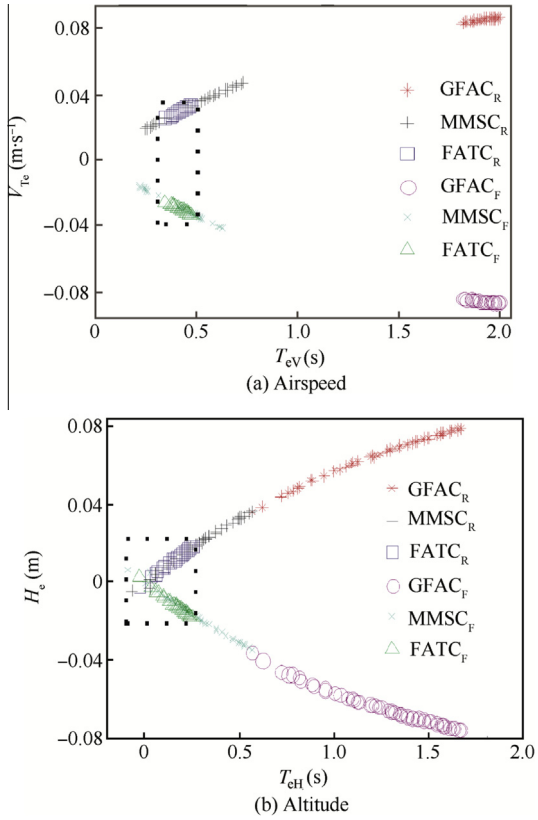

Fig. 9 Statistic results of tracking errors for all test points.

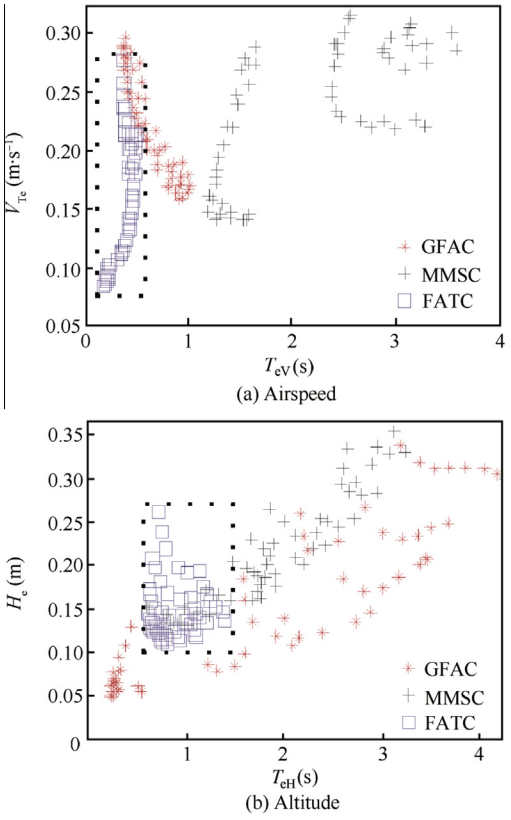

Fig. 10 Statistic results of uncertainties attenuation for all test points.

restrains the airspeed errors within a small range (0.025, 0.034) m/s and the response time errors within (0.35 s, 0.48 s), and so as to the altitude. During (10 s, 15 s), the SMMC guarantees stability at the cost of response performances, so the imposed uncertainties render long adjustment times and large tracking errors, while the GFAC eliminates the airspeed errors quickly but the attenuation qualities of the altitude errors do not represent obvious advantage. The FATC attenuates the induced airspeed and altitude errors within 0.28 m/s and 0.26 m with the adjustment times less than 0.5 s and 1.42 s, and it shows the best uncertainties attenuation performance. Hence, the proposed FATC guarantees consistent and satisfactory tracking performances within the full envelope in spite of uncertainties, and it attenuates the influences of instant uncertainties without sacrificing the response performances.

4.2. Tracking performances under continuous flight over large envelope span

As shown in Fig. 5, the flight trajectory over a large span is designed to verify the tracking performances under a continuous flight in the presence of uncertainties. We select three navigation points to identify the desirable command of the flight state. The trimmed states for three navigation points (A, B and C) in the absence of uncertainties are illustrated in Table 4.

The UAV is initiated at operating point A and switches to point B and C at 5 s and 200 s respectively through filter dynamic

$$G(s) = 0.0009/(s^2 + 0.057s + 0.0009)$$

and then we can obtain the given inputs V_{Tg}, H_{g}:

$$V_{\mathrm{Tg}} = \begin{cases} V_{TA} & t < 5\ \mathrm{s} \\ V_{TB} + (1 - G(s))(V_{TA} - V_{TB}) & 5\ \mathrm{s} \leqslant t < 200\ \mathrm{s} \\ V_{TC} + (1 - G(s))(V_{TC} - V_{TB}) & 200\ \mathrm{s} \leqslant t \leqslant 400\ \mathrm{s} \end{cases}$$

$$H_{\mathrm{g}} = \begin{cases} H_A & t < 5\ \mathrm{s} \\ H_B + (1 - G(s))(H_A - H_B) & 5\ \mathrm{s} \leqslant t < 200\ \mathrm{s} \\ H_C + (1 - G(s))(H_C - H_B) & 200\ \mathrm{s} \leqslant t \leqslant 400\ \mathrm{s} \end{cases}$$

where V_{TA}, V_{TB}, V_{TC} are the airspeeds at points A, B, and C, respectively and H_A, H_B, H_C are the corresponding altitudes.

We introduce sine time-varying parametric perturbation uncertainties defined as $A_{\mathrm{m}} \sin(2\pi(t - t_0)/T)$, where the amplitudes A_{m} for $C_{L\alpha}$, $C_{L\delta_e}$, C_{D0}, A, C_{M0}, C_{Mq}, x_{cgR}, x_{caR} are determined as in Table 3, the imposed time t_0 = 10 s, and the periods T are 30 s, 35 s, 40 s, 45 s, 50 s, 55 s, 60 s, and 80 s, respectively. The failures of 30% reduction of the thrust

Table 4 Trimmed values for three navigation operating points.

Label	Condition		Trimmed states			
	Ma	H (km)	α(°)	θ(°)	δ_{th} (%)	δ_e(°)
A	0.46	7.40	10.7	10.7	65.6	−2.9
B	1.32	10.60	2.6	2.6	66.6	−2.3
C	1.01	3.40	1.6	1.6	85.6	−1.3

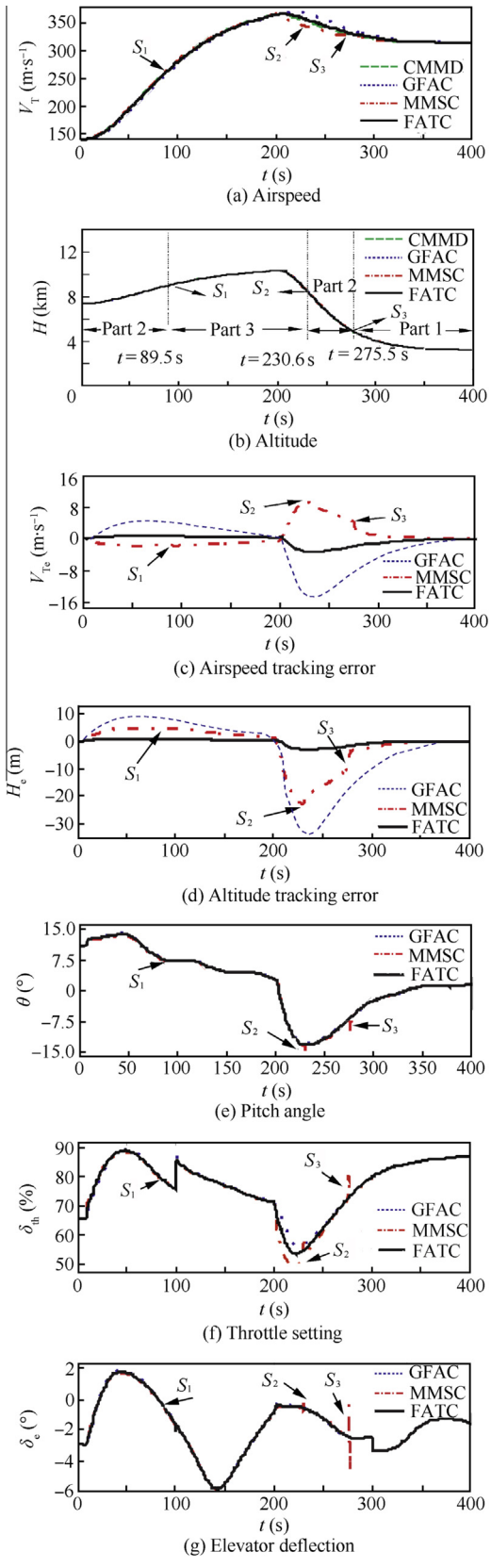

Fig. 11 Responses under continuous flight over a large envelope span.

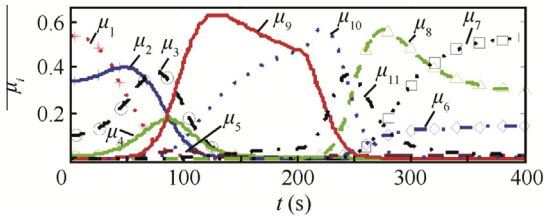

Fig. 12 Membership degrees to 11 fuzzy rules.

and 30% reduction of the elevator effectiveness are imposed at 100 s and 300 s, respectively.

The responses under the continuous flight with the three controllers are shown in Figs. 11 and 12 provides the membership degrees of the UAV to 11 fuzzy rules during the flight process under the feedback control of the FACT.

From Fig. 11, we can conclude that the three controllers all realize stable tracking over the flight under the time-varying uncertainties. After 5 s, the quick decrease of the elevator deflection and the increase of the throttle setting cause the increases of airspeed and altitude. The elevator rises slowly at 8.2 s, and after 48.4 s, the throttle setting declines to relieve the change rates of altitude and airspeed, and then the UAV transforms from increasing to steady-state flight at point *B*. After 200 s, the quick increase of the elevator deflection and the decrease of the throttle setting lead to a quick decline of the UAV. Then the elevator deflection decreases and the throttle setting rises slowly to reduce the difference between the drag and the thrust, so that the UAV transforms from declining to steady-state flight at point *C* gradually. As the aerodynamic drag at point *C* is much larger, the throttle setting reaches a higher value to maintain the balance between the drag and the thrust finally with respect to point *B*. The quick injections of control efficiency failures at 100 s and 300 s cause fast regulations of the elevator and the throttle.

The variations of membership degrees to the 11 fuzzy rules shown in Fig. 12 illustrate the scheduling mechanism of the proposed controller. At any specific moment, the flight condition is subject to 11 fuzzy rules with different membership degrees, which reflect the weights of corresponding local gain matrices. The variations of Mach number and altitude accompanying with the flight over the large envelope span lead to the smooth transition of membership degrees, so the fuzzy multiple Lyapunov function synthesizes the 11 fuzzy Lyapunov matrices $\boldsymbol{X}_j$ with the membership degrees to replace the common Lyapunov matrix $\boldsymbol{X}_c$ and the smooth gain scheduling of the baseline controller of Eq. (15) and the adaptation laws of Eq. (36) can be realized. Therefore, the extra freedom degrees of control parameters are offered.

As shown in Fig. 11, though the three controllers all realize stable tracking, the GFAC embodies the largest tracking errors due to the conservatism compared with the other controllers. Though the MMSC reduces the tracking errors for a certain degree, the relevant tracking performances as shown in Fig. 9 could not be ensured due to the cost of response degradation under the time-varying uncertainties,

and the maximum tracking errors of airspeed and altitude are 9.5 m/s and 23 m, which are obviously larger than 3.5 m/s and 3.3 m caused by the GFAC. Another drawback of the MMSC is also presented, which is the switching between different subsystems. As marked in the altitude curve, three switching processes S_1, S_2, and S_3 are conduced, and they lead to switching dynamics. Especially during S_3, the variation ranges of δ_{th} and δ_e are 11.2% and 4.5°, and they cause the fluctuation of 3.6° for the pitch angle. The switching dynamics degrade the tracking performances and lead to underlying damages. With reduced conservatism and adaptive SHLNN compensation for uncertainties, the FATC ensures stable responses of flight states and guarantees the minimum tracking errors among the three controllers without introducing switching dynamics. Hence, the proposed FATC guarantees satisfactory tracking performances of the desirable commands with strong robustness to the uncertainties during the continuous flight over the large flight envelope.

5. Conclusions

A fuzzy adaptive tracking controller is proposed for the flight of a UAV over a large envelope span in the presence of undesirable uncertainties:

(1) Benefiting from the relaxed conservatism of the fuzzy baseline controller and the adaptation laws, the controller guarantees satisfactory tracking performances of the desirable commands with strong robustness to the uncertainties for the entire flight envelope.
(2) The parameters of the fuzzy baseline controller can be obtained conveniently by solving LMI with reduced computational complexity.
(3) The controller is scheduled based on smooth transition of membership degrees, and the adaptive increment provides continuous compensating signals with bounded parametric eliminates, so the problems of switching dynamics, chattering, and parametric drift are avoided.

References

1. Adams RJ, Buffington JM, Banda SS. Gain scheduled linear PID autopilot for the AIAA controls design challenge aircraft. 1992. Report No.: AIAA-92-4629.
2. Reichert RT. Dynamic scheduling of modern robust control autopilot designs for missiles. *IEEE Control Syst* 1992;**12**(5):35–42.
3. Calise AJ, Lee S, Sharmma M. Development of a reconfigurable flight control law for tailless aircraft. *J Guid Control Dyn* 2001; **24**(5):896–902.

Appendix A. The control parameters for the fuzzy baseline controller

$$N_1 = \begin{bmatrix} -563.86 & 2.89 & -38.52 & 1.35 & -1.03 & 0.15 & 0.03 & -0.96 & 0.76 & 0.13 & -0.13 \\ -37.12 & 8.75 & 1590.8 & 9.89 & -143.9 & 0.21 & -3.68 & -21.3 & 25.14 & -14.70 & -9.76 \end{bmatrix}$$

$$N_2 = \begin{bmatrix} -511.31 & 1.45 & -37.49 & 0.30 & 1.67 & 0.07 & 0.12 & 0.72 & -1.17 & 0.15 & 0.03 \\ 0.18 & 14.39 & 2974.3 & 13.21 & -92.70 & -0.60 & -1.14 & -11.17 & 15.30 & -8.56 & -4.13 \end{bmatrix}$$

$$N_3 = \begin{bmatrix} -660.07 & 1.22 & -35.99 & 0.152 & 3.26 & 0.04 & 0.19 & 1.39 & -1.90 & 0.26 & 0.19 \\ 0.492 & 13.96 & 3965.1 & 11.58 & -80.43 & -0.37 & -0.79 & -7.68 & 10.68 & -7.48 & -2.90 \end{bmatrix}$$

$$N_4 = \begin{bmatrix} -768.52 & 1.29 & -30.64 & 0.19 & 3.82 & 0.041 & 0.22 & 1.64 & -2.22 & 0.28 & 0.22 \\ -2.71 & 15.15 & 4269.2 & 12.08 & -58.86 & -0.39 & 0.34 & 2.43 & -1.85 & -5.89 & -1.10 \end{bmatrix}$$

$$N_5 = \begin{bmatrix} -914.29 & 1.55 & -23.66 & 0.404 & 4.02 & 0.05 & 0.26 & 1.83 & -2.51 & 0.27 & 0.19 \\ -9.55 & 14.28 & 4049.8 & 11.19 & -30.06 & -0.44 & 1.64 & 15.05 & -17.20 & -3.81 & 1.54 \end{bmatrix}$$

$$N_6 = \begin{bmatrix} -1055.5 & 2.47 & -19.41 & 1.25 & 4.28 & 0.03 & 0.42 & 2.59 & -3.62 & 0.22 & 0.02 \\ -20.40 & 9.26 & 3146.5 & 7.14 & 2.74 & -0.34 & 2.70 & 27.46 & -31.96 & -1.30 & 5.24 \end{bmatrix}$$

$$N_7 = \begin{bmatrix} -1215.8 & 7.24 & 29.55 & 5.63 & 3.85 & -0.14 & 1.14 & 5.75 & -8.08 & -0.18 & -0.93 \\ -42.81 & -6.47 & 1111.8 & -5.46 & 39.10 & 0.01 & 3.14 & 38.19 & -44.26 & 2.12 & 10.58 \end{bmatrix}$$

$$N_8 = \begin{bmatrix} -1416.8 & 1.470 & -24.43 & 0.41 & 0.60 & 0.07 & 0.11 & 0.29 & -0.69 & 0.06 & -0.07 \\ -59.05 & -22.99 & 3401.8 & -21.62 & 0.08 & 0.72 & -0.97 & 11.99 & -9.96 & 0.79 & 11.50 \end{bmatrix}$$

$$N_9 = \begin{bmatrix} -1222.1 & 5.20 & -18.1 & 3.85 & -3.60 & -0.01 & 0.34 & 0.21 & -1.08 & -0.51 & -1.24 \\ -70.97 & -30.81 & 1742.3 & -27.24 & -40.23 & 0.605 & -3.66 & -6.15 & 14.31 & -1.35 & 10.15 \end{bmatrix}$$

$$N_{10} = \begin{bmatrix} -1401.5 & 3.28 & -58.88 & 2.085 & -3.98 & -0.02 & 0.10 & -0.87 & 0.58 & -0.40 & -0.88 \\ -73.32 & -37.4 & 3162.8 & -34.38 & -43.04 & 1.26 & -4.885 & -13.98 & 23.81 & -1.17 & 11.20 \end{bmatrix}$$

$$N_{11} = \begin{bmatrix} -1547.4 & 2.47 & -53.37 & 1.33 & -3.14 & 0.01 & 0.04 & -0.861 & 0.69 & -0.27 & -0.65 \\ -87.01 & -49.06 & 3462.4 & -45.18 & -27.96 & 1.84 & -5.43 & -12.50 & 22.79 & 0.85 & 15.20 \end{bmatrix}$$

$$X_1 = \begin{bmatrix} 66.83 & * & & & & \cdots & \cdots & & & & * \\ 1.25 & 0.94 & & & & & & & & & \\ 12.77 & -2.17 & 75.45 & & & & & & & & \\ 0.9100 & 0.86 & -2.53 & 0.80 & & & & & & & \\ -86.78 & 0.65 & 7.20 & -0.63 & 579.76 & \ddots & & & & & \vdots \\ 48.25 & -0.04 & -0.00 & -0.02 & -91.79 & 114.08 & \ddots & & & & \vdots \\ 5.618 & 0.17 & -0.96 & 0.12 & 20.30 & -92.77 & 170.58 & & & & \\ -101.69 & 0.91 & -8.39 & 0.47 & 507.32 & -106.42 & 57.99 & 660.96 & & & \\ 9.521 & -1.27 & 11.38 & -0.74 & -89.23 & 19.62 & -89.73 & -332.51 & 606.3 & & \\ 4.427 & -0.07 & 2.04 & -0.12 & 2.52 & -29.01 & 33.92 & -3.67 & 3.14 & 19.38 & * \\ -1.118 & -0.21 & 0.74 & -0.27 & 14.40 & 3.34 & -7.55 & -49.62 & 62.67 & 2.17 & 30.55 \end{bmatrix}$$

$$X_4 = \begin{bmatrix} 66.86 & * & & & & \cdots & \cdots & & & & * \\ 1.32 & 1.08 & & & & & & & & & \\ 11.05 & -5.44 & 152.32 & & & & & & & & \\ 0.98 & 0.99 & -5.72 & 0.93 & & & & & & & \\ -86.62 & 0.94 & 0.29 & -0.34 & 580.3 & \ddots & & & & & \vdots \\ 48.25 & -0.05 & 0.19 & -0.03 & -91.80 & 114.04 & \ddots & & & & \vdots \\ 5.62 & 0.19 & -1.44 & 0.14 & 20.35 & -92.71 & 170.49 & & & & \\ -101.61 & 1.04 & -11.31 & 0.58 & 507.54 & -106.4 & 57.98 & 660.93 & & & \\ 9.46 & -1.39 & 14.35 & -0.86 & -89.51 & 19.61 & -89.69 & -332.48 & 606.46 & & \\ 4.45 & -0.03 & 1.06 & -0.08 & 2.60 & -28.99 & 33.91 & -3.64 & 3.11 & 19.38 & * \\ -1.10 & -0.17 & -0.21 & -0.23 & 14.48 & 3.33 & -7.53 & -49.55 & 62.59 & 2.19 & 30.59 \end{bmatrix}$$

4. Wang J, Hovakimyan N, Cao CY. Verifiable adaptive flight control: unmanned combat aerial vehicle and aerial refueling. *J Guid Control Dyn* 2010;**33**(1):75–87.
5. Theodoulis S, Duc G. Missile autopilot design: gain-scheduling and the gap metric. *J Guid Control Dyn* 2009;**32**(3):986–96.
6. Saussie D, Sady L, Akhrif O, Berard C. Gain scheduling with guardian maps for longitudinal flight control. *J Guid Control Dyn* 2011;**34**(4):1045–59.
7. Marcos A, Bennani S. LPV modeling, analysis and design in space systems: rationale, objective and limitations. 2009. Report No.: AIAA-2009-5633.
8. Kharisov E, Hovakimyan N, Wang J, et al. L1 adaptive controller for time-varying reference systems in the presence of unmodelled nonlinear dynamics. *Proceedings of 2010 American Control Conference*; 2010 June 30–July 02; Baltimore, MD. Piscataway, NJ: IEEE; 2010. p. 886–91.
9. Wang XF, Hovakimyan N. L1 adaptive controller for nonlinear time-varying reference systems. *Syst Control Lett* 2012;**61**(4):455–63.
10. Huang YQ, Sun CY, Qian CS, Wang L. Non-fragile switching tracking control for a flexible air-breathing hypersonic vehicle based on polytopic LPV model. *Chin J Aeronaut* 2013;**26**(4):948–59.
11. Lu B, Wu F, Kim SW. Switching LPV control of an F-16 aircraft via controller state reset. *IEEE Trans Control Syst Technol* 2006;**14**(2):267–77.
12. Hou YZ, Wang Q, Dong CY. Gain scheduled control: switched polytopic system approach. *J Guid Control Dyn* 2011;**34**(2):623–8.
13. Huang XY, Wang Q, Wang YL, Hou YZ. Adaptive augmentation of gain-scheduled controller for aerospace vehicles. *J Syst Eng Electr* 2013;**24**(3):272–80.
14. Oosterom M, Babuska R. Design of a gain-scheduling mechanism for flight control laws by fuzzy clustering. *Control Eng Pract* 2006;**14**(7):769–81.
15. Hu X, Wu L, Hu C, Gao H. Fuzzy guaranteed cost tracking control for a flexible air-breathing hypersonic vehicle. *IET Control Theory Appl* 2012;**6**(9):1238–49.
16. Li HY, Yu JY, Hilton C, Liu HH. Adaptive sliding mode control for nonlinear active suspension vehicle systems using T–S fuzzy approach. *IEEE Trans Ind Electr* 2013;**60**(8):3328–38.
17. Jiang B, Gao ZF, Shi P, Xu YF. Adaptive Fault-tolerant tracking control of near-space vehicle using Takagi–Sugeno fuzzy models. *IEEE Trans Fuzzy Syst* 2010;**18**(5):1000–7.
18. Feng G. $H\infty$ controller design of fuzzy dynamic systems based on piecewise Lyapunov functions. *IEEE Trans Syst Man Cybernet B Cybernet* 2004;**34**(1):283–92.

19. Tanaka K, Hori T, Wang HO. A multiple Lyapunov function approach to stabilization of fuzzy control systems. *IEEE Trans Fuzzy Syst* 2003;**11**(4):582–9.
20. Bouarar T, Guelton K, Manamanni N. Robust fuzzy Lyapunov stabilization for uncertain and disturbed Takagi–Sugeno descriptors. *ISA Trans* 2010;**49**(4):447–61.
21. Wise KA, Lavretsky E, Hovakimyan N. Adaptive control of flight: theory, application, and open problems. *Proceedings of 2006 American Control Conference*; 2006 June 14–16; Minneapolis, MN. Piscataway, NJ: IEEE; 2006. p. 5966–71.
22. Wu TZ, Juang YT. Design of variable structure control for fuzzy nonlinear systems. *Expert Syst Appl* 2008;**35**(3):1496–503.
23. Stevens BL, Lewis FL. *Aircraft control and simulation*. 2nd ed. New York: Wiley; 2003.
24. Zhang ML. *Flight control system*. Beijing: National Defense Industry Press; 1994 [Chinese].
25. Wang LX, Mendel JM. Fuzzy basis functions, universal approximation, and orthogonal least-squares learning. *IEEE Trans Neural Netw* 1992;**3**(5):807–14 [Chinese].
26. Liu Z, Wang Y. Fuzzy robust tracking control within full envelope for unmanned aerial vehicle. *Journal of Beijing University of Aeronautics and Astronautics* 2014;**40**(6):762–8.
27. Juang CF, Lin CT. An online self-constructing neural fuzzy inference network and its applications. *IEEE Trans Fuzzy Syst* 1998;**6**(1):12–32.
28. Volyanskyy KY, Haddad MM, Calise AJ. A new neuroadaptive control architecture for nonlinear uncertain dynamic systems: beyond σ and e modifications. *IEEE Trans Neural Netw* 2009;**20**(11):1707–23.
29. Tuan HD, Apkarian P, Narikiyo T, Yamamoto Y. Parameterized linear matrix inequality techniques in fuzzy control system design. *IEEE Trans Fuzzy Syst* 2001;**9**(2):324–32.
30. Khalil HK. *Nonlinear systems*. 3rd ed. Upper Saddle River: Prentice-hall; 2002.
31. Yu L. *Robust control—LMI approach*. Beijing: Tsinghua University Press; 2002 [Chinese].

Liu Zhi is currently a Ph.D. candidate in navigation, guidance and control at Beihang University (BUAA), China. He received his B.S. degree in automatic control from Xiamen University, Xiamen, China in 2008. His current research interests include fuzzy adaptive control of complex systems, application of advanced control to aerospace, conversion control of VTOL UAVs, and flight control of UAVs with large envelopes.

Wang Yong received his B.S., M.S., and Ph.D. degrees in navigation, guidance and control from Beihang University (BUAA), China in 1988, 1990, and 2001, respectively. In 2001, he joined the Unmanned Aerial Vehicle Research Institute at BUAA. He has taken part in lots of national major projects, and has been responsible for the flight control system design for advanced UAVs. He is the Assistant Chief Engineer and senior technical follow in the Unmanned Aerial Vehicle Research Institute at BUAA. Since 2009, he has been a professor affiliated with navigation, guidance and control at BUAA. His main research field includes advance control theory and its application in flight control engineering, flight control of multi-model vehicles, and autonomous flight management and control system of intelligent UAVs.